nature communications



Article

https://doi.org/10.1038/s41467-025-64110-w

Homeostasis of glucose and lipid metabolism during physiological responses to a simulated hypoxic high altitude environment

Received: 30 April 2024

Accepted: 8 September 2025

Published online: 24 October 2025

Check for updates

Yi Lin ^{1,2,3,4}, Bingyu Li ^{1,2,4}, Xinying Shi ^{1,2,3,4}, Yangkang Chen^{1,2}, Shengkai Pan ^{1,2,3}, Zhenzhen Lin^{1,2,3}, Zhongru Gu ^{1,2,3}, Frank Hailer ^{3,5}, Li Hu ^{2,3,6} ≪ Xiangjiang Zhan ^{1,2,3,7} ≪

Homeostasis facilitates maintenance of physiological processes despite extrinsic fluctuations. In aerobic organisms, homeostasis is mainly fueled by metabolism of glucose and lipids, and requires oxygen as a metabolic substrate. Lack of oxygen can therefore trigger an imbalance of homeostasis in vivo. How animals living at high altitude hypoxic conditions can maintain homeostasis between the two types of metabolism remains largely unknown. Here, we establish a 'falconized' mouse model based on an adaptive *EPAS1* genetic variant identified from saker falcons (*Falco cherrug*) on the Qinghai-Tibet Plateau (QTP). We show that homeostasis between glucose and lipid metabolism in the liver under chronic hypoxia is maintained in male falconized mice. This homeostasis is mediated by genetic factors and behavioral plasticity, resulting in higher survival rates even under acute hypoxia than wild type mice. Our study highlights a key role of metabolic homeostasis maintenance for survival in extreme environments, and provides potential targets for the treatment of associated metabolic diseases.

Homeostasis, the maintenance of stable physiological conditions in vivo through self-regulation, is crucial for an organism's survival¹. When organisms are exposed to external stressors, this homeostasis can be disrupted. To counteract such disruption, organisms display a range of transient and reversible physiological and behavioral responses to recover internal stability^{2,3}. These responses require energy, e.g., for up-regulation of biochemical reactions⁴. Across eukaryotes, metabolism of glucose and lipids represents the two main pathways for meeting such energetic demands⁵.

High altitude habitats (above 2500 m) are characterized by reduced oxygen partial pressures, which pose severe physiological and metabolic challenges to aerobic organisms^{6,7}. To cope with the stress imposed by hypoxia, organisms such as birds^{8,9}, humans^{10,11}, and other mammals^{12,13} exhibit a range of adaptations and responses to maintain oxygen homeostasis. These include physiological responses like higher hemoglobin-oxygen affinity, enhanced oxygen saturation, and improved cardiovascular function⁸⁻¹³. These adaptations and responses help maximize oxygen delivery to tissues under low-oxygen conditions.

¹State Key Laboratory of Animal Biodiversity Conservation and Integrated Pest Management, Institute of Zoology, Chinese Academy of Sciences, Beijing, China. ²Key Laboratory of Animal Ecology and Conservation Biology, Institute of Zoology, Chinese Academy of Sciences, Beijing, China. ³Cardiff University - Institute of Zoology Joint Laboratory for Biocomplexity Research, Chinese Academy of Sciences, Beijing, China. ⁴University of the Chinese Academy of Sciences, Beijing, China. ⁵Organisms and Environment, School of Biosciences, Cardiff University, Cardiff, Wales, UK. ⁶Key Laboratory of Coastal Biology and Biological Resources Utilization, Yantai Institute of Coastal Zone Research, Chinese Academy of Sciences, Yantai, China. ⁷Center for Excellence in Animal Evolution and Genetics, Chinese Academy of Sciences, Kunming, China. ⊠e-mail: lihu@yic.ac.cn; zhanxi@ioz.ac.cn

In addition to these physiological changes, metabolic reprogramming also plays a crucial role in facilitating efficient oxygen utilization under hypoxia¹⁴. Reduced oxygen availability triggers alterations in cellular metabolism, particularly in glucose and lipid utilization, as the body adjusts to meet energy requirements, with potentially dramatic consequences for fitness and survival^{15,16}. Although glucose metabolism requires less oxygen per mole of ATP synthesized and thus is more oxygen-efficient than lipid metabolism¹⁷, animals living at high altitudes exhibit different metabolic strategies. For example, mammals native to high altitude environments such as the Tibetan antelope (Pantholops hodgsonii) and American pika (Ochotona princeps) preferentially metabolize glucose¹⁸. On the other hand, some small high altitude endothermic animals maintain their thermogenic capacity mainly by mobilizing lipids, which exhibited a higher energy density (e.g., deer mice (Peromyscus maniculatus)19 and ground tits (Parus humilis)20, but see Andean mice (Phyllotis andium and P. xanthopygus)²¹ for exceptions).

However, how animals living at high altitudes maintain homeostasis between the two types of metabolism remains largely unknown, as does whether metabolic homeostasis could play any role in facilitating their persistence under hypoxia. Most previous studies explored glucose metabolism or lipid metabolism separately, or were restricted to only one energy source and pathway. However, glucose and lipid are not metabolized independently, but rather are coregulated in the glucose-fatty acid cycle^{22,23}. Hence, if one metabolism mode is up- or down-regulated, the balance between the two metabolism modes could become disrupted, risking metabolic damage²⁴ or oxidative stress from reactive oxygen species (ROS)²⁵. Important aspects of the co-regulation of glucose and lipid pathways and the organismal responses to hypoxic stress are therefore not yet fully understood. One main reason for the lack of information on this is the absence of a suitable animal model that would allow the study of interactions between glucose metabolism and lipid metabolism of animals under hypoxic versus normal conditions. To address this, we designed an in vivo experiment and predicted that the balance between glucose metabolism and lipid metabolism may play a key role during organismal responses to high altitude-induced hypoxia.

EPAS1 (endothelial PAS domain protein 1, also known as hypoxiainducible factor 2α (HIF2 α)) is a regulatory gene recently identified in a range of vertebrate species to be critical for adaptation to low-oxygen conditions on the Qinghai-Tibet Plateau (QTP)²⁶⁻²⁸. Under normoxia, EPAS1 is hydroxylated by prolyl hydroxylase (PHD), triggering its ubiquitination by von Hippel-Lindau protein (pVHL) and subsequent degradation. In contrast, under hypoxia, the regulatory function of EPAS1 is initiated through the formation of heterodimers with the aryl hydrocarbon receptor nuclear translocator (ARNT) via the Per-Arnt-Sim domain, then HIF downstream pathways can be activated (e.g., metabolism, angiogenesis)29. As a key transcription factor, EPAS1 regulates pathways involved in both glucose and lipid metabolism³⁰⁻³², EPAS1 is therefore an ideal candidate for investigation of the cellular mechanisms that enable the maintenance of metabolic homeostasis under hypoxic stress. This gene is involved in the development of diabetes and obesity^{33,34} as well as high altitude associated syndromes, such as hypoxemia³⁵, polycythemia³⁶, anorexia³⁷ and other cardiovascular or respiratory diseases³⁸. Previous studies on species on the QTP have identified adaptive *EPAS1* variations in humans²⁶, mammals³⁹, birds²⁸ and snakes⁴⁰, but no studies to date have investigated the impact of the QTP fixed or dominant variants on both metabolic pathways jointly. Here, we developed knock-in mice containing a specific EPAS1 mutation found in high altitude-adapted saker falcons recent colonizers of the QTP⁹-to study the co-regulation of glucose and lipid metabolism in animals experimentally exposed to hypoxic conditions. Through physiological, transcriptome and metabolome analyses of this animal model, we discover that homeostasis between glucose and lipid metabolism under hypoxia is maintained in adapted, knock-in mice, but not in the wild type. We further uncover a range of genetic and behavioral mechanisms that contribute to persistence and survival under hypoxic conditions. Finally, we present evidence that the regulatory effects of the falcon-derived *EPAS1* mutation in mice also apply to wild saker falcons on the QTP. Our study highlights the contribution of metabolic homeostasis to increased survival under hypoxia, and also provides a potential therapeutic target for the treatment of glucose and lipid metabolism disorders.

Results

Physiological and key metabolic characteristics of *EPAS1*^{V162T/V162T} falconized mice under hypoxia

To explore homeostatic regulation patterns between glucose and lipid metabolism in animals in hypoxic environments, we knocked a saker falcon-derived variant²⁸ into the *EPAS1* gene of C57BL-6J mice, using a CRISPR-Cas9 approach⁴¹. The mutant was obtained by editing AC into GT in Exon 5 of the mouse *EPAS1* gene on chromosome 17, changing Valine (Val) to Threonine (Thr) for the 162th amino acid residual (Fig. 1a; Supplementary Fig. 1). Resulting knock-in ('falconized') mice and their offspring were genotyped and verified by Sanger sequencing (Fig. 1a). In this study, we used homozygous mutant mice (*EPAS1*VI62T,' 'falconized') as the experimental group, since this is the predominant genotype identified in the QTP saker population⁹.

We investigated energy mobilization (glucose or lipid) in homozygous mutant (EPASI^{V162T}/V162T) and wild type mice (EPASI^{+/+}), when exposed to 1) normal O2 concentrations (normoxia; 21% O2, observed at sea level⁴²), and 2) hypoxic conditions (hypoxia; 10% O₂; equivalent of > 5000 m above sea level⁴²). We then measured the respiratory exchange ratio (RER; carbon dioxide production divided by oxygen uptake) for each tested mouse before and after each hypoxic treatment, to study the shift in substrate utilization by using a TSE metabolic cage system⁴³ (**Methods**). We found that mutant and wild type mice had the same RER patterns under normoxia (RER of around 0.75; Supplementary Fig. 2). In contrast, the patterns were distinct under hypoxic conditions: mutant mice maintained a significantly higher RER compared to wild type mice (Fig. 1b). In addition, we observed no consistent change over time in RER in mutant mice (RER values fluctuating around 0.75 with no significant signal of decline) between hypoxic and normoxic conditions (Fig. 1c), in contrast with wild type mice which exhibited a trend of decreasing RER across the seven days (Fig. 1d). These results suggest a stable ratio in substrate utilization of glucose and lipid in response to hypoxia in falconized mice, while the lower and decreasing RER in wild type mice suggests a shift in energy utilization from glucose to lipids44.

Given that our mutant mice demonstrated similar RER values before and after hypoxic treatment at each time point (Fig. 1c), we hypothesized that the maintenance of metabolic homeostasis in mutant mice is achieved by balancing glucose metabolism and lipid metabolism. To test this, we performed a widely targeted metabolomics/lipidomics analysis on mouse hepatic tissue samples, using the ultra-performance liquid chromatography and tandem mass spectrometry (UPLC-MS/MS)⁴⁵ to quantify the carbohydrate and lipid metabolites at different hypoxic treatment intervals: normoxia (day 0; DO), early hypoxia (days 2-4; D2-D4), and late hypoxia (day 7; D7). An orthogonal partial least squares-discriminant analysis (OPLS-DA) of carbohydrate and lipid metabolites clearly separated mutant from wild type mice throughout the duration of hypoxic treatments (Supplementary Figs. 3 and 4), as did a principal component analysis (PCA) (Supplementary Figs. 5 and 6). These results indicate distinct carbohydrate and lipid metabolism landscapes in the two types of mice under hypoxic conditions.

We then examined hepatic carbohydrate levels in both types of mice and found that the total content of glucose exhibited a common turning point from decline to recovery on D3 (Fig. 2a). However, under hypoxic conditions, mutant mice gained hepatic glucose more quickly

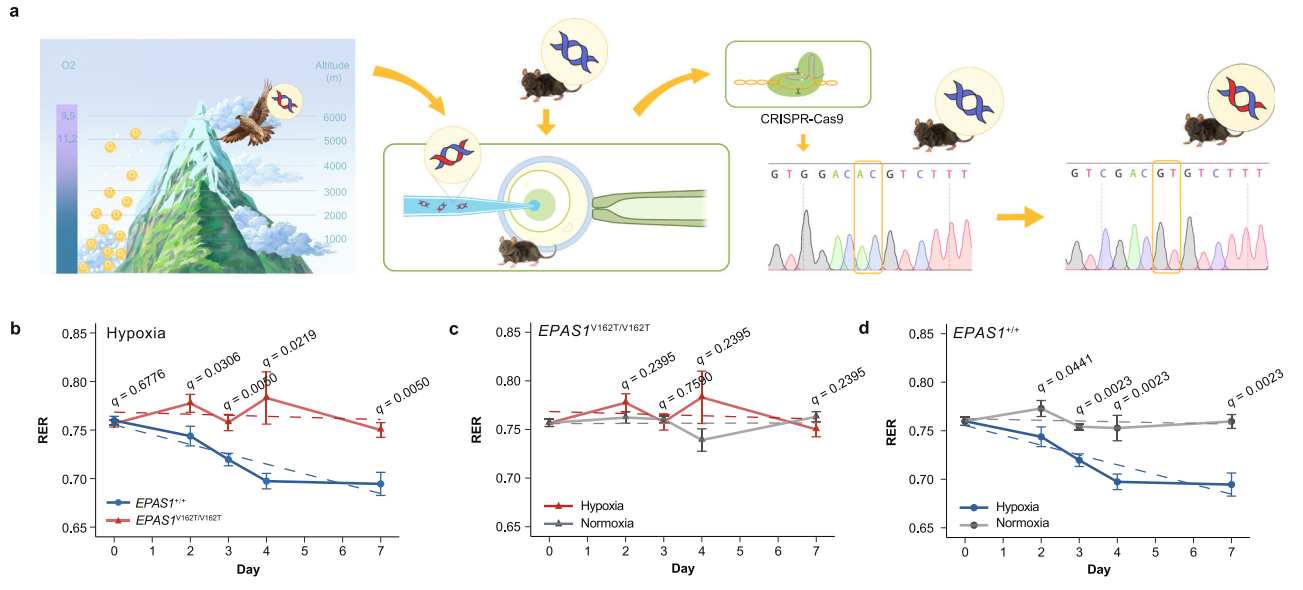


Fig. 1 | **Physiological characteristics of** *EPASI*^{V162T}/V162T **falconized (mutant) mice under hypoxia. a** Genetically engineered knock-in (falconized) mice and their verification by Sanger sequencing. **b** Comparison of respiratory exchange ratio (RER) in $EPASI^{V162T}/V162T$ (n=10 on D2, 3, 7 and n=9 on D4) and $EPASI^{+/+}$ (n=10 on D2, 3, 4 and n=11 on D7) mouse individuals under hypoxia. Two-sided Welch's t test was applied for the testing on D4 and two-sided t tests for the remaining. Mixed linear model analysis (dotted line) revealed significantly lower RER in the wild type (p=1.57E-06). **c,d** RER measurements for $EPASI^{V162T}/V162T$ (n=10 on D2, 3, 7 and n=9 on D4) and $EPASI^{+/+}$ (n=10 on D2, 3, 4 and n=11 on D7) mouse individuals under

hypoxia and normoxia, respectively. Two-sided paired Welch's t test was applied for the testing on D3 and D4 in mutant mice and two-sided paired t tests for the remaining. Regression analysis (dotted line): p = 0.931, $R^2 = 9.79$ E-05 in mutant mice under normoxia; p = 0.845, $R^2 = 5.08$ E-04 in mutant mice under hypoxia; p = 0.726, $R^2 = 1.55$ E-03 in wild type mice under normoxia; p = 1.35E-11, $R^2 = 0.437$ in wild type mice under hypoxia. q values in (\mathbf{b} - \mathbf{d}) represent p values adjusted by multiple test correction (FDR method). The bars display mean \pm SD. Source data are provided as a **Source Data** file.

and recovered after D3 to a similar level as they previously had under normoxia, in contrast with consistently reduced hepatic glucose contents observed in wild type mice (Fig. 2a). We also observed that the mutant mice maintained a higher hepatic glucose level than wild type mice under hypoxia (Fig. 2a), consistent with the results obtained from the targeted metabolomics analysis (Supplementary Fig. 7). To verify whether the mutant mice possessed a higher capacity to regulate hepatic glucose under hypoxic conditions on D3, we conducted a glucose tolerance test (GTT) on both types of mice under hypoxic conditions on that day. As expected, we found that mutant mice maintained significantly lower blood glucose levels than wild type mice (Fig. 2b; q = 0.0143; at 15 min), despite the administration of glucose during the GTT, while there was no significant difference between the two mouse types under normoxia.

We next compared lipid contents in the livers of each mouse type, and found that abundances of most free fatty acids (FFAs) were recovered after D3 or D4 to a similar level as under normoxia (D0) in mutant mice (14/22; Supplementary Figs. 8 and 9), agreeing well with the hepatic glucose recovery time point (Fig. 2a). In contrast, abundances of most FFAs in wild type mice (21/30) were significantly higher under hypoxia than initially on DO, and remained elevated after D3 or D4 (e.g., Dodecanedioic acid, Tetradecanedioic acid, FFA (12:0); Supplementary Figs. 8 and 10), which supports our conclusion that wild type mice have a lipid-biased energy utilization (e.g., Fig. 1d). Similarly, we found that wildtype mice had higher FFA levels than mutants under hypoxia (e.g., Dodecanedioic acid, Tetradecanedioic acid, FFA (12:0); Fig. 2c; Supplementary Fig. 11), and this result was in agreement with that from the targeted metabolomics analysis (Supplementary Fig. 12). Because triglycerides (TGs) can be hydrolyzed into FFAs for energy production²³, we then examined the number of differentially expressed TG types between mutant and wildtype mice. As expected, we found that wild type mice had a higher lipid level than mutant mice when faced with hypoxic stress: among the 41 subclasses of lipid metabolites that were significantly altered between the two mouse types, TG was the main subclass of differential lipid metabolites (Supplementary Fig. 13), especially on D3 (235 among 374 lipid metabolites, 62.83%) (Fig. 2d; Supplementary Fig. 14). Furthermore, the relative abundance of TGs was significantly lower in mutant mice (Fig. 2e; Supplementary Fig. 15), and correspondingly higher in wild type mice.

Genetic mechanism balancing the homeostasis of glucose and lipid metabolism

An amino acid substitution experimentally introduced into EPAS1 thus generated unique hypoxic metabolism responses in mutant mice, enabling us to study the genetic and physiological mechanisms underlying the maintained balance between the metabolism of glucose and lipid fuels. In these falconized mice, the Val to Thr substitution in the PAS domain (Exon 5) is expected to increase hydrophilicity of EPAS1, thus reducing its binding affinity to the ARNT, then affecting its interaction with pVHL.

To test this, we performed co-immunoprecipitation (Co-IP) assays to evaluate the protein-protein interactions between EPAS1 and ARNT, as well as EPAS1 and pVHL. The EPAS1V162T/V162T and EPAS1+/+ were constructed with pCDNA3.1-EGFP vectors and expressed in Hela cells, respectively. A western blot assay revealed a stable expression in both types (Supplementary Fig. 16), suggesting that the point mutation had no influence on the expression of EPAS1. The myc-tagged EPAS1 and flag-tagged ARNT were then co-expressed in the Hela cells and 293T cells, respectively, to assess their interaction. Our Co-IP experiment demonstrated that the EPAS1 mutant had a weakened proteinprotein interaction with ARNT compared to that of the wild type in either cell line (Fig. 3a; Supplementary Fig. 16), suggesting that the mutation reduces the binding affinity of EPAS1 to ARNT. Further Co-IP experiment from the co-expression of myc-tagged EPAS1 and flagtagged pVHL in 293T cells revealed that the EPAS1 mutant exhibited a stronger protein-protein interaction with pVHL compared to the wild type (Supplementary Fig. 16). These results, together, suggested that

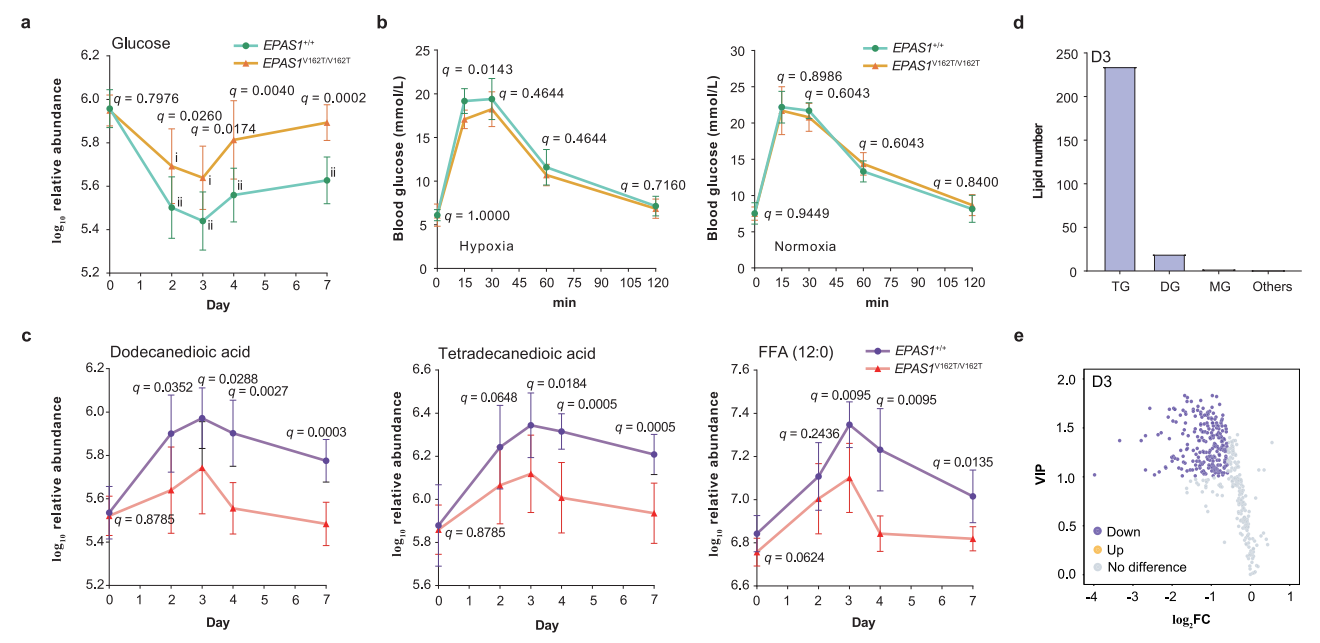


Fig. 2 | **Glucose and lipid metabolic characteristics of** *EPASI*^{VI62T} *Falconized* **(mutant) mice under hypoxia. a** Changes in glucose content in hepatic samples of mutant (i) and wild type (ii) mice in comparison with their control group (DO), and the differences between the two types of mice at each time point (iii). i: D2 vs DO (q = 0.0025), D3 vs DO (q = 0.0025); ii: D2, 3, 4 or 7 vs DO (q = 0.0002; 1.11E-06; 5.86E-06; 1.37E-05); iii: q values were labeled at each time point. Two-sided Mann-Whitney U tests were applied for the testing: D3 vs DO in mutant mice; D2 vs DO in wild type mice; D2 and D3 between the two mouse types. Two-sided t tests were applied for the remaining tests (t = 8 for each group). **b** Glucose tolerance test under hypoxia and normoxia on D3 (t = 9 for each group). A two-sided t test was applied. **c** Changes in free fatty acids contents in hepatic samples and the differences between mutant and wild type mice at each time point. Two-sided Mann-Whitney U tests were applied for the testing: D0, 2 and 4 (dodecanedioic acid); D0

and D2 (Tetradecanedioic acid); D0 (FFA (12:0)). Two-sided Welch's t tests were applied for the testing of FFA (12:0) on D4 and D7. Two-sided t tests were applied for the remaining tests (n = 8 for each group). t The lipid number of differentially expressed lipid metabolites between mutant and wild type mice on D3. The number means the number of differentially expressed lipid metabolite subclasses detected between the two types of mice. TG: Triglyceride, DG: Diacylglycerol, MG: Monoacylglycerol. t Volcano plots of differential abundance of triglycerides between mutant and wild type mice on D3. The t-axis is the fold change (log₂FC), and t-axis is the variable important in projection (VIP). A down-regulated metabolite was determined by VIP t 1 and FC t 0.67. t values in t 1 and t 2 values adjusted by multiple test correction (FDR method). The bars display mean t 5D. Source data are provided as a **Source Data** file.

the EPAS1 mutant exhibited reduced interaction with ARNT and increased interaction with pVHL, supporting our hypothesis about a blunted function of *EPAS1* in the falconized mice.

In addition, polymorphisms of the *HIF* genes may affect their gene expression profiles⁴⁶. To test this, we identified five full-length transcripts of the *EPAS1* gene using the Iso-seq data from the pooled liver samples (**Methods**), and compared transcript expression differences between mutant and wild type mice using the RNA-seq data at different hypoxic time points (D0, D2, D3, D4, D7). Our results showed that the dominant transcript (accounting for more than 90% of *EPAS1* expression, Supplementary Fig. 17) was significantly down-regulated on D3 in mutant mice compared with wildtype mice (Supplementary Fig. 18; Supplementary Data 1). Low expression of *EPAS1* has previously been implicated in mammalian responses to low oxygen stress^{26,47}.

As a key eukaryotic transcription factor, the mutated *EPAS1* is predicted to have widespread effects on the complex gene expression networks associated with carbohydrate and lipid metabolism in the falconized mice. To investigate this, we applied a differential gene regulatory network analysis to look for differences in the expression landscape between the mutant and wild type mice using the transcripts obtained from our RNA-seq data (**Methods**), and found that the mutated *EPAS1* affected the regulation of genes involved in both metabolic pathways under hypoxic conditions (Supplementary Fig. 19).

To elucidate these regulation mechanisms more precisely, we firstly identified all the differentially expressed genes (DEGs) between each experimental group and normoxic controls from the whole RNA-seq data for mutant and wild type mice, respectively (Supplementary Data 2 and 3). Among genes in the glucose metabolic pathways, we

found that the Gck expression, a key rate-limiting enzyme gene in glycolysis, was significantly down-regulated in mutant mice on either D2 or D3, but recovered (a similar expression level as D0) since D4 (Fig. 3b; Supplementary Figs. 20 and 21). In addition, both the Gys2 and Ugp2 that are involved in glycogen synthesis consistently exhibited upregulated expression, suggesting a potential for hepatic glycogen accumulation in mutant mice (Fig. 3b; Supplementary Figs. 20 and 21). In contrast to the mutants, wild type mice under hypoxic conditions showed generally up-regulated expression of G6pc, which functions as antagonistic enzyme of Gck (Fig. 3b; Supplementary Figs. 20 and 22). As a rate-limiting enzyme in gluconeogenesis, an elevated expression of G6pc suggests that the wildtype mice may have compensated for the shortage of glucose via mobilizing lipids through gluconeogenesis, in response to hypoxic stress. Furthermore, our metabolomic analysis showed the relative abundance of two thirds carbohydrate metabolites in mutant mice was recovered to a normoxic level since D4, in contrast to being only three recovered in wild type mice (Fig. 3b, c; in green; Supplementary Data 4 and 5), resulting in significantly higher relative abundance of carbohydrate metabolites in mutant than wild type mice under hypoxia (Supplementary Fig. 23; Supplementary Data 6). These elevated carbohydrate metabolite levels in mutant mice could result from relatively sufficient substrate supply (e.g., glucose) for metabolism under oxygen stress.

From all the identified DEGs (Supplementary Data 2 and 3), our KEGG enrichment analysis further found that in both types of mice under hypoxia, DEGs were enriched in pathways such as fatty acid degradation and metabolism (Supplementary Figs. 24 and 25). We then examined those DEGs identified in the FFA metabolic pathways and found that the genes exhibited variable up- and down-regulation in

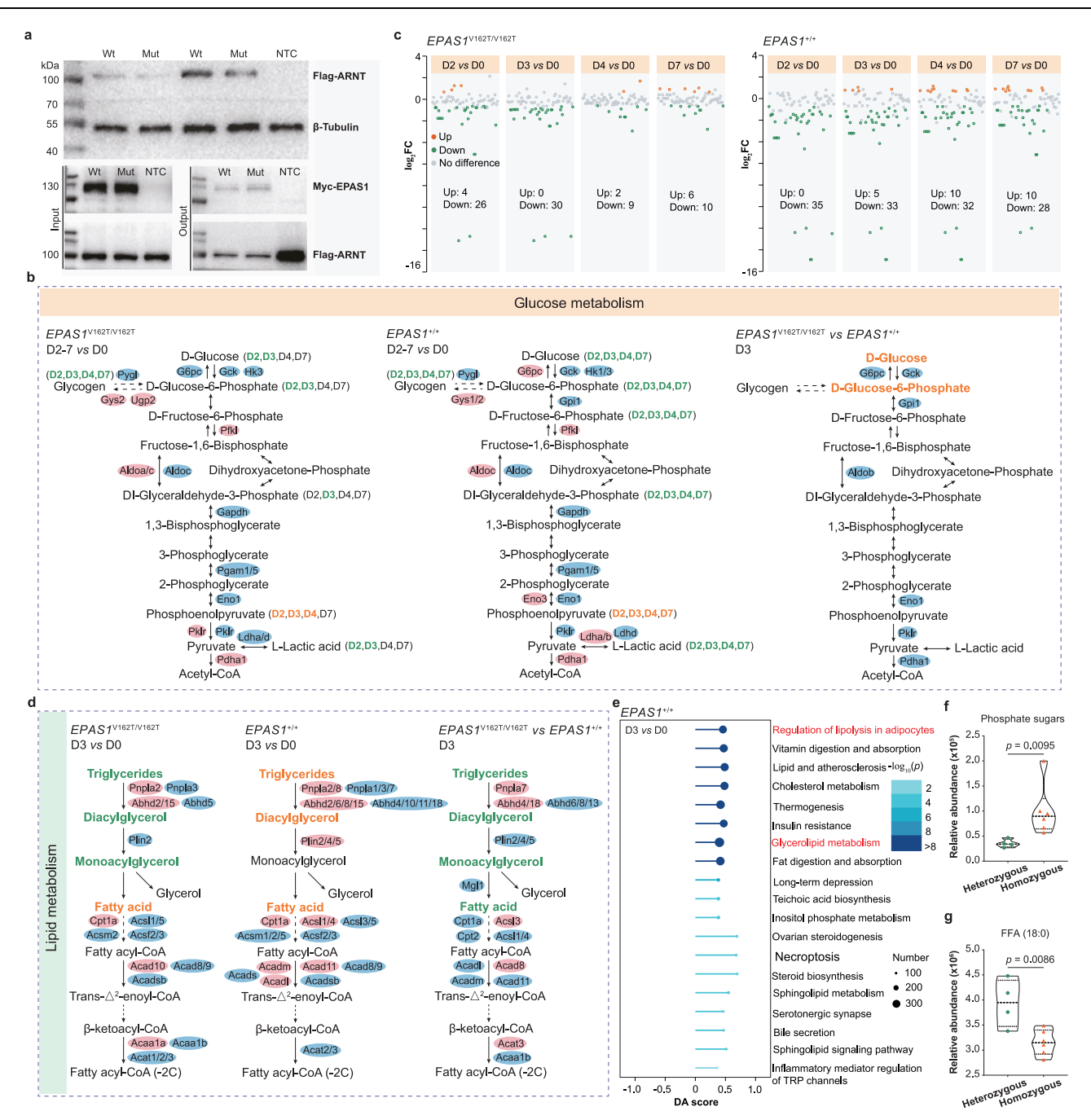


Fig. 3 | Genetic mechanism underlying the homeostasis of glucose and lipid metabolism. a Interaction between the EPAS1 VI62T (Mut: mutant) or EPAS1 VI62T (Wt: wild type) protein and ARNT protein was detected by a co-immunoprecipitation assay with the β -Tublulin as internal control. Each experiment was repeated independently three times. NTC: negative control. b Summary statistic on significantly up-/down-regulated liver genes or metabolites in the glucose metabolic pathways between each of testing points and DO, and those between the two mouse types on D3. Up- and down-regulated genes are in pink and blue, respectively. Up- and down-regulated carbohydrate metabolites are in orange and green, respectively. c Volcano plots of differentially expressed carbohydrate metabolites in mutant and wild type mice under hypoxia in comparison with DO, respectively. The *y*-axis is fold change (log₂FC). Significance was determined by

having a variable important in projection value \geq 1, and FC being \geq 1.5 or FC \leq 0.67. **d** Summary statistic on significantly up-/down-regulated liver genes or metabolites in the lipid metabolic pathways between D3 and D0, and those between the two mouse types on D3. The symbols are the same as Fig. 3b. **e** KEGG pathways of all differentially expressed lipid metabolites in wild type mice on D3 in comparison with D0. Differential abundance (DA) score: a normalized value ranging from -1 to 1 that represents the overall regulatory trend of the pathway. Circles represent the number of metabolites enriched in the pathways. Raw *p* values were used. **f.g** Carbohydrate and lipid contents in plasma samples of wild saker falcons with different *EPAS1* genotypes. The bars show mean \pm SD. A two-sided Mann-Whitney U test and a two-sided *t* test were used. Source data are provided as a **Source Data** file.

each mouse type (Fig. 3d; Supplementary Figs. 21, 22 and 26; Supplementary Data 7 and 8). However, the number of DEGs in wild type mice was always higher than that in mutants, regardless of hypoxic treatment intervals, suggesting a relatively active metabolic reprogramming of lipid metabolism in wild type mice (Supplementary Fig. 27).

For example, the *Plin4*, *Plin5* (involved in lipid accumulation^{48,49}) and *Acsl1* (involved in initial step of FFA β -oxidation⁵⁰) genes were always significantly up-regulated in wild type mice during hypoxic treatments in comparison with DO, suggesting high potential for lipid accumulation and FFA utilization in the wild type liver (Fig. 3d; Supplementary

Figs. 22 and 26). Supporting evidence for this conclusion comes from our metabolomic analysis of liver lipid metabolites: in wild type mice exposed to hypoxia, our KEGG enrichment analysis found that the differentially expressed lipid metabolites were significantly enriched in lipolysis pathways from D3 to D7 (e.g., regulation of lipolysis in adipocytes, glycerolipid metabolism; Fig. 3e; Supplementary Fig. 28), with a generally higher number of up-regulated lipid metabolites along with the hypoxic treatment compared to the normoxic control (Supplementary Fig. 29).

In addition, we have also checked whether glucose and lipid metabolic DEGs between different testing points and normoxia within the same mouse type were also differentially expressed between the two mouse types at the focal testing points (D3-D7) (Supplementary Data 2, 3 and 9). As a result, we found a large overlap between the two DEG datasets (41/68 in either mouse type, 41/44 between mouse types) (Supplementary Table 1). Notably, we found consistent results in the key DEGs in the glucose (*G6pc* and *Gck*) and lipid (*Plin4*, *Plin5* and *Acsl1*) metabolic pathways on the focal days (Figs. 3b and 3d; Supplementary Figs. 30, 31 and 32), suggesting a true difference between genotypes.

Since there is an association between the *EPAS1* mutation and a relatively lower abundance of lipid metabolites in mutant mice compared to wildtype mice (Supplementary Fig. 33; Supplementary Data 10), we further used RNA interference (RNAi) to check the effect of a blunted *EPAS1* function on lipid metabolism. Specifically, we knocked down the *EPAS1* gene expression in 293T cells to simulate the scenario observed in mutant mice (Fig. 3a), and our qPCR results showed that genes involved in lipolysis (e.g., *ACSL1*)⁵¹ and lipogenesis (e.g., *FASN*, *IDH1*)^{51,52} were all down-regulated in the lipid metabolism, including *IDH1*, which mediates reductive glutamine metabolism for lipogenesis (Supplementary Fig. 34).

Given that the *EPASI*^{v162T}V162T mutation is derived from saker falcons inhabiting the QTP, we checked whether wild sakers have similar metabolic characteristics as found in the knock-in (falconized) mice. Through the analysis of blood samples of QTP sakers possessing the same *EPASI* allele (six homozygotes versus four heterozygotes for the *EPASI* mutation conveying adaptation to hypoxia)²⁸, we found a significantly higher relative abundance of carbohydrates (Fig. 3f), but a significantly lower relative abundance of FFAs in the homozygote than heterozygote sakers (Fig. 3g). These results are consistent with our observations in mutant mice (e.g., glucose in Fig. 2a; FFA in Fig. 2c and Supplementary Fig. 11), and strongly support our finding that this mutation can regulate the homeostasis of glucose and lipid metabolism under hypoxia in falconized mice and tentatively also in sakers inhabiting the QTP.

Behavioral plasticity during glucose and lipid metabolism homeostasis

Besides genetic changes involved in adaptation, human and other animals also display behavioral regulations when faced with hypoxic stress^{53,54}. Oxygen saturation is one of the main indicators of hypoxia status in the body⁵⁵. In our study, we found that arterial oxygen saturation has a similar decrease in either type of mice under hypoxia (Supplementary Fig. 35), indicating that both groups experienced hypoxic stress. Humans and other animals adjust respiratory patterns (e.g., increased breathing rate) to counteract hypoxic stress^{53,54}; they help attenuate the effects of reduced oxygen availability. We therefore, together with oxygen saturation measurements, measured the daily breathing rate under hypoxia along a time series (D0, D2, D3, D4, D7) using the MouseOx Plus system (Starr Life Science). As expected, both mutant and wild type mice exhibited an increase in the breathing rate during early hypoxia compared to normoxic treatments (D0) (Fig. 4a). However, relative to D0, the breathing rate in mutant mice always increased significantly on D2, D3 or D4, whereas wild type mice increased on D3 or D4 (Fig. 4a). A more sensitive breathing rate in mutant mice may lead to a higher supply of oxygen to the blood even under hypoxic conditions, contributing to glucose and lipid metabolism homeostasis.

We also compared other behavioral traits (food intake, defecation and locomotion) which have been implicated in the glucose and lipid metabolism 9,56,57 . We observed that both types of mice exhibited reduced food intake and defecation initially, followed by a recovery trend (Fig. 4b, c). Differently, whereas both types of mice decreased their activities in hypoxic treatments, mutant mice showed a relatively lower reduction in general locomotion under hypoxia, due to their already lower activities under normoxia (Fig. 4d, q = 4.59E-05). We further compared the behavioral differences between the two mouse types across hypoxic treatments by ANOVA, and found significant differences in either food intake (Fig. 4b, p = 0.0369) or locomotor activity (Fig. 4d, p = 3.04E-05). These alterations in feeding (energy input) and locomotion (energy output) of the mutant mice could potentially change the content of substrates for glucose and lipid metabolism.

To disentangle the relative contributions of behavioral plasticity, environment and genetics to maintenance of glucose and lipid metabolic homeostasis in mutant mice, we formulated a Structural Equation Model (SEM; Methods) to quantify their influences on RER, a proxy for metabolic homeostasis (Fig. 1c). First, we conducted PCA using four behavioral variables: breathing rate, food intake, food absorption ((1-(fecal mass/ food intake)) *100) and locomotion. We found that the first principal component (PC1) explained 57.65% of the variance (Supplementary Table 2), so we then integrated this component as a combinational behavioral variable for downstream SEM modeling (**Methods**). Our simulations showed that besides a significantly positive effect of the genetic mutation on RER under hypoxia (coef. = 0.63, p = 5.55E-08; Fig. 4e), the behavior also changed in response to hypoxic treatments (coef. = 0.85, p = 2.13E-11; Fig. 4e) and impacted RER in a positive manner (coef. = 0.59, p = 8.46E-03; Fig. 4e). These results provide evidence that behavioral adjustments can also contribute significantly to the maintenance of glucose and lipid metabolic homeostasis in a low oxygen environment.

Evolutionary benefits of the glucose and fat metabolism homeostasis

Weight loss in humans and other animals under hypoxia is thought to be caused by multiple factors, such as the energy imbalance of the two main nutrients (glucose and lipids)⁵⁸ and dehydration⁵⁹. We therefore monitored the changes in body weight of EPAS1V162T/V162T mice and wildtype mice, respectively, under normoxic and hypoxic conditions for seven days. As expected, both mouse types had a stable body weight under normoxia, but the hypoxic treatments caused a decrease in body mass during the first two days, followed by a recovery in the remaining days (Fig. 5a). This is a typical response observed for animals under hypoxia⁶⁰. Then, we compared the differences in body weight change trends between the two mouse types across hypoxic treatments, and found that they were significantly different (Fig. 5a, p = 0.0391) and in comparison with the wild type, the mutant mice demonstrated relatively higher body weight from D2 to D4. Body weight recovery may result from the response of metabolic regulation. To investigate whether changes in metabolites (e.g., hepatic glucose or FFA) contributed to body weight recovery, we performed a correlation analysis between body weight and hepatic metabolites. As expected, we found that body weight change was significantly positively correlated with glucose metabolites and negatively correlated with lipid metabolites (Supplementary Fig. 36). High hepatic glucose usually promotes glycogen storage, increasing lipogenesis and leading to increased fat storage and weight gain⁶¹⁻⁶³. Furthermore, since being underweight is associated with a higher mortality in humans⁶⁴, a quicker recovery of body weight in falconized mice under hypoxia may convey survival benefits. In addition, since it is found that dehydration led to an increase in hematocrit (HCT) under hypoxia⁶⁵, we used the

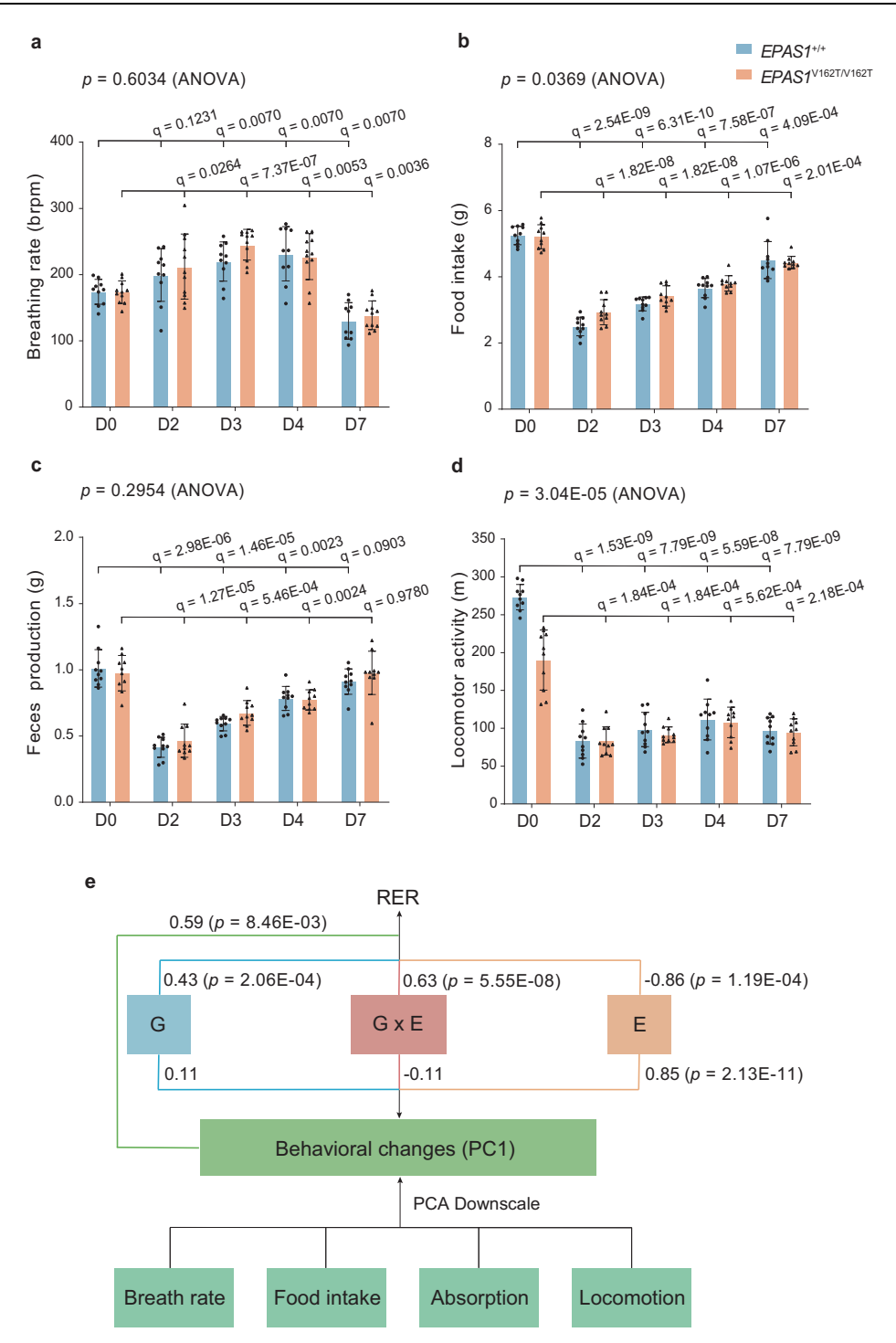


Fig. 4 | **Effects of behavioral plasticity on homeostasis of glucose and lipid metabolism. a**–**d** Comparisons of breathing rate ($EPASI^{V162T,V162T}$, n = 11; $EPASI^{+/+}$: n = 10), food intake (n = 10 for each group), fecal production (n = 10 for each group), and locomotor activity (n = 10 for each group) between each of the testing point (D2, 3, 4 or 7) and D0 for the $EPASI^{V162T,V162T}$ and $EPASI^{+/+}$ mouse individuals, respectively. The bars show mean \pm SD. Two-sided paired t tests and two-way

repeated measures ANOVA with corrections were applied. Q values represent p values adjusted by multiple test correction (FDR method) and were labeled on the top of each hypoxic testing point. **e** Contributions of behavioral plasticity, environment and genotype of $EPASI^{VI62T/VI62T}$ mice to respiratory exchange ratio (RER) using a structural equation simulation. Source data are provided as a **Source Data** file.

HCT as a proxy to evaluate the dehydration state in the tested mice. Our results showed that, while both mouse types exhibited elevated HCT values under hypoxia, no significant differences were observed at any time points between the two mouse types (Supplementary Fig. 37). Our analysis, thus, suggests comparable levels of dehydration in both mouse types under hypoxic treatments, although the actual water

balance mechanism during these body weight changes warrants future efforts.

Another likely detrimental consequence of imbalanced glucose and lipid metabolism is the accumulation of ROS within cells, which can shorten individual life span²⁵. In our study, we examined the expression levels of genes involved in the ROS metabolic pathway

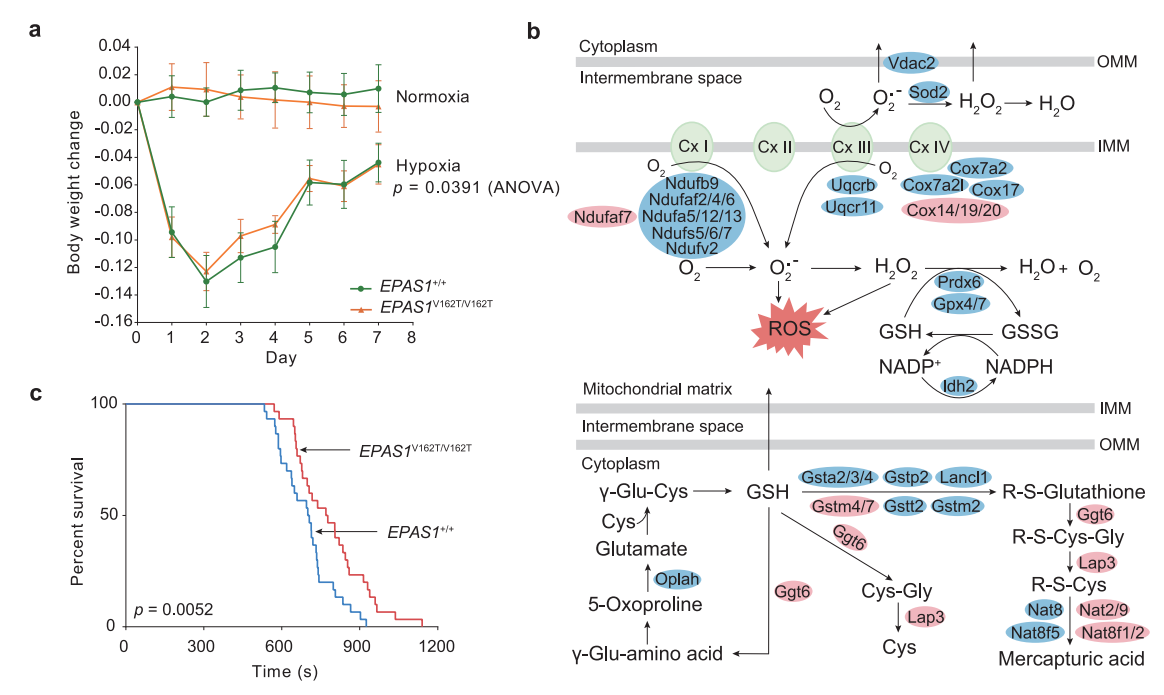


Fig. 5 | **Organismal benefits of homeostasis of glucose and lipid metabolism. a** Body weight changes in $EPASI^{VI6ZIT/VI6ZIT}$ and $EPASI^{+/+}$ mouse individuals under normoxia ($n=13\ vs\ 11$) and hypoxia (n=10 for each group). The bars show mean \pm SD. Two-way repeated measures ANOVA with corrections was applied. **b** Differential expression levels of genes playing a role in reactive oxygen species (ROS) metabolism in falconized mice compared to wildtype mice. Up- and down-regulated genes are in pink and blue, respectively. GSH: Glutathione, GSSG:

oxidized Glutathione, γ-Glu-Cys: γ-Glutamyl-Cysteine, γ-Glu-amino acid: γ-Glutamyl-amino acid, Cys: Cysteine, Cys-Gly: Cysteinyl-Glycine, R-S-Cys-Gly: R-S-Cysteinyl-Glycine, R-S-Cys-Cysteine. Cx: Complex, OMM: Outer membrane, IMM: Inner membrane. \mathbf{c} Comparison of survival rates between $\mathit{EPAS1}^{V162T,V162T}$ (n=30) and $\mathit{EPAS1}^{V1}$ (n=30) mouse individuals under acute hypoxia (4% O_2) based on the Kaplan-Meier survival analysis. Source data are provided as a **Source Data** file.

among all the identified DEGs (Supplementary Data 9) using the RNA-seq data, and found that most of the genes were significantly down-regulated in the *EPAS1*^{V162T/V162T} mice under hypoxic treatment in comparison with wild type mice (in blue, Fig. 5b). Predicted to limit the overproduction of ROS, this down-regulation suggests that falconized mice may have experienced a lower oxidative stress under hypoxia, presumably with beneficial effects on their survival.

To test whether a single *EPAS1* mutation could indeed result in higher survival in mutant mice, we first pre-acclimated the two types of mice under gradient hypoxic conditions (**Methods**), allowing for metabolic reprogramming, then exposed them to lethal hypoxic conditions (4% O_2)^{13,66,67} and monitored their heart rates with the MouseOx system. In both types of mice, the heart rate dropped rapidly, but the mutant mice had a longer survival time (785.4 \pm 25.4 s) in contrast with wild type (695.3 \pm 19.0 s) under the same acute hypoxic conditions (Supplementary Fig. 38). A Kaplan-Meier survival analysis confirmed that the overall survival rate of mutant mice was significantly higher than that of the wild type (Fig. 5c). Our experiments therefore revealed that falconized mice were more tolerant to hypoxia extremes.

Discussion

Metabolic changes have been reported for both residential and migratory animals living on the QTP¹⁴. However, previous studies of the genetic basis of metabolic response to hypoxia and hence adaptation to QTP conditions have only focused on a single metabolic pathway at a time (either glucose or lipid), despite these two main pathways being coregulated^{22,23}. One reason for the lack of studies investigating both pathways in vivo has hitherto been the absence of a suitable animal model. Given that *EPAS1* is one of the master genes regulating both metabolic pathways⁶⁸, we here established a mouse model with an *EPAS1* genetic variant originally identified in high

altitude-adapted saker falcons from the QTP. We find that falconized mice expressing this variant were able to maintain glucose and lipid metabolic homeostasis in a low oxygen environment (Fig. 1c), unlike their wild type, lowland counterparts for which we observe a lasting shift towards lipid metabolism (Fig. 1d). Our analyses of physiological, gene expression and metabolomics show that the maintenance of metabolic homeostasis in falconized mice mainly resulted from a greater capacity to balance the two main types of fuel metabolism after hypoxic exposure (e.g., Figs. 1c, 3b and d). These findings illustrate a critical role of the EPAS1 gene for organismal persistence in high altitude hypoxic environments, mediated by a previously unknown key role of EPAS1 in maintenance of homeostasis of glucose and lipid metabolism. Besides genetic changes, the contribution of behavioral plasticity should not be overlooked. Energy-associated behavioral regulation also has an important role in metabolic homeostasis maintaining (Fig. 4e). Thus, findings from our falconized mouse model have uncovered a novel metabolic contribution to high altitude response that goes beyond a simple genetic basis. However, it is noted that we were unable to conduct the same experiments (e.g., RER, hepatic metabolites) in wild saker falcons due to the constraints imposed by the endangered status of this species. Therefore, the homeostasis maintenance mechanism of glucose and lipid metabolism in native plateau animals in the wild warrants future research.

The obtained insights highlight that tissue oxygen utilization towards complex metabolic responses is essential for maintaining homeostasis of glucose and lipid metabolism, contributing to coping with high altitude hypoxia. Through a mouse model, we identified a metabolic mechanistic that facilitates this homeostasis in vivo, through joint regulation of the gene expression landscape that relates back to the *EPAS1* gene (Supplementary Fig. 19). *EPAS1* does by directly regulating the expression of key genes or network involved in metabolism and its related downstream pathways (e.g., vascular endothelial

growth factor B (VEGFB) pathway^{24,69}) to ensure a coordinated response to balance the metabolism under hypoxia. In this study, we found that the mutant *EPAS1* allele conveyed a decrease in the gene function (e.g., a lower protein affinity with ARNT (Fig. 3a), a decreased expression level on D3 (Supplementary Fig. 18)), consistent with other species displaying blunted responses to hypoxia^{40,47}. Reduced EPAS1 gene function can attenuate VEGF-induced angiogenesis (e.g., downregulated *Vegfa* and *Vegfb*; (Supplementary Table 3; Supplementary Data 9)), helping to maintain functional blood vessels for oxygen delivery⁷⁰ and then contributing to metabolic homeostasis. Furthermore, inhibitors of EPAS1 are being investigated in clinical trials for cancer treatment, and evidence has emerged that HIF also plays a major role in metabolic imbalance diseases⁷¹. For example, overexpression of HIF2α aggravates nonalcoholic fatty liver disease progression⁷², while inhibition of HIF2 α decreases the metabolic adverse phenotypes⁶⁸. The key enzyme-encoding genes (e.g., Gck and Acsl1) that we here show to be regulated by the QTP-derived EPAS1 genetic variant have been reported previously as prognostic biomarkers for metabolic diseases^{73,74}, although their synergistic roles in homeostasis of glucose and lipid metabolism are unclear. Thus, our finding of an EPAS1 genetic variant that is adaptive at high altitude and that increases an organism's ability to maintain metabolic homeostasis provides a possible avenue for this gene to be used as a potential drug target in the treatment of relevant metabolic diseases.

Methods

Ethics statement

All animal experiment procedures were under the guidance of the Ethics Committee of Institute of Zoology, Chinese Academy of Sciences (NO. SYXK Jing 2021-0063), China. The collection and processing of mouse tissue and saker falcon plasma samples used in this study were approved by the Institutional Animal Care and Use Committee of Institute of Zoology, Chinese Academy of Sciences, China.

Generation of falconized mice

The falconized mice were generated by CRISPR/Cas9-based technology. Briefly, based on the alignment to a positive selected exonic mutation of EPAS1 in the QTP saker falcon²⁸, we selected the sgRNA target sequence (5'-CCGAGCGTGACTTCTTCATG-3') of C57BL/6 J background murine EPAS1 to direct Cas9-mediated cleavage. After microinjection into mouse zygotes, the transgenic engineered mouse was genotyped by polymerase chain reaction (PCR) with genomic DNA extracted from a toe tip sample from each mouse. We established two independent falconized mouse lines using the above method: one mainly used for experiments and the other only for validation purposes. The heterozygous mice (*EPAS1*^{+/V162T}) were then crossed to obtain mutant homozygous (EPAS1^{V162T}/V162T) and wild type mice (EPAS1^{+/+}). Male mice (8-9 weeks old) were used for all the physiological, behavioral and molecular experiments because female physiological status may periodically fluctuate and bias the metabolism analysis⁷⁵. Before experiments, all mice were maintained in a specific pathogen free environment at 23 °C ±1 °C and 40-60% humidity under 12:12-hour light/dark cycles and provided ad libitum with water and rodent chow (Beijing Keao Xieli Feed Co., Ltd., Cat. 1016706476803973120).

DNA extraction and sequencing

The mouse toe tip samples were digested in 500 μ l lysis buffer (10 mM Tris-HCl, 10 mM EDTA (pH 8.0), 100 mM NaCl, and 0.5% SDS) with 15 μ l proteinase K (Macklin) and incubated at 56 °C in a thermo-shaker (Allsheng) until the tissues had been dissolved. The DNA was precipitated with 2-Propanol BioReagent (Sigma) and pelleted by centrifugation, washed with 75% (vol/vol) Ethyl alcohol (Sigma), and dissolved in 100 μ l DNase/RNase-Free Water (Solarbio). For genotyping, the DNA extract was used to perform PCR amplification to amplify a 170 bp product, followed by Sanger sequencing (Forward primer: 5′-

TTAATTTAACTGGCTCCCACGCC-3'; Reverse primer: 5'-CTCCAC-GAATCCTACCTTCC-3'). To check potential off-target effects, we designed PCR primers (Supplementary Data 11) for the potential off-target sites predicted by CRISPOR⁷⁶, and verified potential mutations (exons and introns) in the parental mice used for breeding through PCR and Sanger sequencing (Supplementary Figs. 39 and 40).

Hypoxic chamber for mouse maintenance

A normobaric hypoxic chamber was used to maintain a stable hypoxic environment during the process of animal experiments. The chamber was composed of an incubator, a transfer bin and an oxygen concentration monitoring/control system (Attendor). The transfer bin was used for transferring mice, water, food, and bedding materials, and ensures a stable environment in the hypoxic chamber. The system regulated and maintained the hypoxic environment through nitrogen, and the precision of oxygen concentration control was \pm 0.1%. Since it is found that most QTP sakers are homozygous for the mutated *EPAS1* allele (derived allele frequency around 80%)⁹, we used *EPAS1* mice as the experimental groups. The mutant and wild type mice were exposed to 10% O₂ and 4% O₂ in the incubator for chronic and acute hypoxia experiments, respectively.

Measurements of the respiratory exchange ratio

EPAS1^{+/+} and EPAS1^{VI62T/VI62T} male mice were randomly split into four groups, with each group analyzed at different treatment time points: 1) D2 (10 vs 10), 2) D3 (10 vs 10), 3) D4 (10 vs 9) and 4) D7 (11 vs 10). We measured the RER of each experimental mouse before and after the hypoxic treatments using a Labmaster caging system (TSE). Dry air flowed through each sealed cage at a speed of 0.7 L/min and then into the gas analyzer at a speed of 0.39 L/min. Oxygen and carbon dioxide concentrations were measured after drying. The RER was recorded and calculated using the Labmaster software (TSE). Both types of mice were fasted and maintained at 30 °C for 3 h without food during the experiment. Three continuous RER values were obtained at the lowest oxygen consumption recorded: these were averaged and used as the resting RER⁴³. After measurements, mice were euthanized using a high dose of CO₂, and liver samples were collected and stored at -80 °C.

An additional independently derived knock-in mice for validation purposes were randomly split into two groups ($10\ vs\ 10$ on D3 and D4, respectively) to verify the RER results using the same measurement method as described above, and the results were the same (Supplementary Fig. 41).

Simple linear regression (using the Im function in *R* package 'stats' (version 4.2.1)⁷⁷) was used to examine whether RER changed significantly over the seven-day hypoxic treatment across the four groups defined by genotype (*EPAS1**)¹ or *EPAS1**1062T, and treatment condition (normoxia or hypoxia). To evaluate whether there were differences between the two genotypes under hypoxic treatments, a linear mixed-effects model was applied using the 'Ime4' package (version 1.1.35.1) in R^{78} , with genotype and time as the fixed effects and individual as a random effect.

Measurements of hematocrit

Blood samples were collected from $EPASI^{*/+}$ and $EPASI^{V162T/V162T}$ mice using EDTA-anticoagulant vacuum tubes (BD Biosciences) after the hypoxic treatments (n = 7 vs 6 on D2, 12 vs 7 on D3, 9 vs 8 on D4 and 5 vs 8 on D7) and normoxic control (11 vs 12 on D0). The HCT was measured using a Mindray BC-2600Vet blood routine analyzer (Mindray).

Measurements of body mass

Male mice (8–9 weeks old) were randomly housed in normoxic ($EPASI^{+/+}$, n=10; $EPASI^{V162T/V162T}$, n=10) and 10% O₂ conditions ($EPASI^{+/+}$, n=10; $EPASI^{V162T/V162T}$, n=10) with free access to water and standard rodent chow. Body weight (BW) of each mouse was measured daily

from D0 to D7. The body weight change was calculated as: $(BW_{dayX} - BW_{day0}) / BW_{day0}$, where "X" varied from 1 to 7 (days).

Correlation analysis on the body weight and metabolite changes through linear mixed-effects modeling

We analyzed the correlation between body weight and hepatic metabolite changes (e.g., glucose and FFA) over seven days in the experimental mice using mixed linear models. The mean body weight change was set as the dependent variable, the mean metabolite abundance as the fixed effect, and the tested genotype as a random effect. All continuous variables were standardized (mean = 0, SD = 1) before modeling. The analysis was fitted using the *R* language package 'lme4'.

Measurements of food intake and fecal production

A total of ten $EPASI^{*/+}$ and ten $EPASI^{V162T/V162T}$ male mice were housed individually. Food intake for each cage was calculated under normoxic conditions (D0) by subtracting the remainder of food and the spilled food in the cage from the original amount offered. The two groups of mice were then housed in $10\% O_2$ conditions and food intake data were collected in the same way at D2, D3, D4, D7, respectively. Total production of feces was also collected at D0, D2, D3, D4, D7 for each individual.

Locomotor activity, oxygen saturation and breathing rate measurements

Experimental mice ($EPASI^{+/+}$, n=10; $EPASI^{V162T,V162T}$, n=10) were kept separately under normoxia and hypoxia, and their activities were recorded using a camera (Hikvison). Their locomotion was analyzed using EthoVision XT16 video tracking system (Noldus).

We measured the arterial oxygen saturation and breathing rate of mice using the collar clip in a MouseOx Plus pulse oximeter (STARR Life Science). An area of hair around the neck of each mouse (11 mutant and 10 wild type mice) was shaved three days prior to treatment in order to provide an area for the oximeter to contact the skin. After mice acclimated to the clip, they were monitored in a non-invasive manner and the oxygen saturation and breathing rate were recorded in real-time under normoxic (D0) and hypoxic (D2, D3, D4 and D7) conditions.

Glucose tolerance test in mice

The $EPASI^{+/+}$ (n=9) and $EPASI^{VI62T/VI62T}$ (n=9) male mice were fasted overnight before intraperitoneal (IP) injections of glucose (Sigma) (2 g kg⁻¹ body weight). Blood was taken from the tail vein before the IP injections and at 0, 15, 30, 60, and 120 min after injections under normoxia (DO), and under hypoxia on D3. Glucose levels were measured for each sample using a glucometer (Roche).

Total RNA isolation from liver samples of *EPAS1*^{+/+} and *EPAS1*^{V162T}/V162T mice

Each liver sample stored at $-80\,^{\circ}\text{C}$ was thawed on ice and cut into small pieces ($<1\,\text{cm}^3$) on a petri dish. After randomly multi-point sampling on the dish⁷⁹, 20 mg liver sample was selected and placed in a 1.5 ml Eppendorf tube. 1 ml TRIzol reagent (Invitrogen) was added and the mixture homogenized at $4\,^{\circ}\text{C}$. RNA extractions were performed according to the manufacturer's protocol (Invitrogen), combining the mixture with chloroform (Sinopharm), collecting the supernatant and finally precipitation using 2-propanol and washing with 75% ethanol. Finally, the pellet was dissolved with DNase/RNase-free water and stored at $-80\,^{\circ}\text{C}$.

Cell culture

Hela cells (ATCC) and 293T cells (ATCC) were cultured in Dulbecco's modified Eagle's medium (Gibco) supplemented with 10% fetal bovine serum (Gibco) and 1% Penicillin-Streptomycin (P/S) (Gibco) at 37 °C in a

humidified 5% $\rm CO_2$ incubator (Thermo Fisher Scientific). Cells were passaged using DPBS (Gibco) and 0.25% Trypsin-EDTA (Gibco).

EPAS1 protein expression assay in vitro

Complete *EPAS1* cDNA sequences were synthetized by the PrimeScript reverse transcriptase (Takara) and PCR-amplified using oligonucleotides (Forward primer: 5'- GGCTTAAGATGACAGCTGACAAGGAGAA –3'; Reverse primer: 5'- ATACCGGTATGGTGGCCTGGTCCAGAGC –3'). The cDNA (*EPAS1*^{+/+} and *EPAS1*^{VI62T}/NI62T) and *pCDNA3.1-EGFP* vector (ZOMANBIO, Cat. ZK430) were digested with AfIII and Agel enzymes for cloning, using products first verified by Sanger sequencing.

The plasmids *pCDNA3.1-EGFP-EPAS1, pCDNA3.1-EGFP-EPAS1mut* and *pCDNA3.1-EGFP* were transfected into Hela cells using Lipofectamine 2000 (Invitrogen) following the manufacturer's instructions, and the transfected cells were cultured under normoxia (21% O_2) and hypoxia (1% O_2), respectively. After 48 h, the transfected cells were collected and stored at $-80\,^{\circ}\text{C}$.

The expression level of EPAS1 protein was quantified in vitro by Western blotting. The proteins were extracted from cell lysates using RIPA lysis buffer (Thermo Fisher Scientific) with protease inhibitors (Thermo Fisher Scientific) and the concentrations were determined using a BCA kit (Thermo Fisher Scientific). The proteins were separated using SDS-PAGE and transferred to a PVDF membrane (GE Healthcare). The membranes were blocked with 5% skimmed milk for 1 h at room temperature and incubated with primary antibodies (Anti-GFP antibody (1: 5,000, Abcam, ab183734) and β -Actin Monoclonal antibody (1: 10,000, Gene-Protein Link, P01L03)) at 4 °C overnight, then incubated with secondary antibodies (Goat Anti-Rabbit IgG-HRP (1: 10,000, Gene-Protein Link, P03S02S) and Goat Anti-Mouse IgG-HRP (1: 10,000, Gene-Protein Link, P03S01S)) at room temperature. The target proteins were detected using the ChemiDoc MP system (Bio-Rad).

Co-IP experiments of EPAS1 and ARNT protein, EPAS1 and VHL protein

The complete *EPASI* cDNA sequences were amplified by PCR using oligonucleotides (Forward primer: 5'- GGCTTAAGATGACAGCTGA-CAAGGAGAA –3'; Reverse primer: 5'- CCGCTCGAGGGTGGCCTGGTC-CAGAGC –3'). The cDNA (*EPASI**/+ and *EPASI**/162T/N162T) and *pCDNA3.1-3*×*Myc-C* vector (MiaoLingBio, Cat. P14395) were digested with AfIII and Xhol enzymes for cloning. The complete *ARNT* cDNA sequences were PCR-amplified using oligonucleotides (Forward primer: 5'-CGGCTAGCATGGCGGCGACTACAGCTAA –3'; Reverse primer: 5'-CGGAATTCTTCGGAAAAGGGGGAAACA –3'). The complete *VHL* cDNA sequences were PCR-amplified using oligonucleotides (Forward primer: 5'-CGGCTAGCATGCCCCGGAAGGCAGCCAG –3'; Reverse primer: 5'-CGGAATTCAGGCTCCTCTTCCAGGTGCT –3'). The *ARNT* and *VHL* cDNA and *pCDNA3.1-FLAG-C* vector (MiaoLingBio, Cat. P11108) were digested with NheI and EcoRI enzymes for cloning, followed by a verification using Sanger sequencing.

The plasmids *pCDNA3.1-3×Myc-C-EPAS1*, *pCDNA3.1-3×Myc-C-EPAS1mut* and *pCDNA3.1-3×Myc-C* were co-transfected with *pCDNA3.1-FLAG-C-ARNT* into Hela cells or 293T cells. The plasmids *pCDNA3.1-3×Myc-C-EPAS1*, *pCDNA3.1-3×Myc-C-EPAS1mut* and *pCDNA3.1-3×Myc-C-EPAS1*, *pCDNA3.1-3×Myc-C-EPAS1mut* and *pCDNA3.1-3×Myc-C-EPAS1* were co-transfected with *pCDNA3.1-FLAG-C-VHL* into 293T cells, respectively. After 48 hrs, the transfected cells were washed using DPBS and lysed with Mag c-Myc IP/Co-IP Buffer-1 (Thermo Fisher Scientific), and the protein concentration was determined using a BCA kit. We performed the immunoprecipitation using Pierce Magnetic c-Myc-Tag IP/Co-IP Kit (Thermo Fisher Scientific) according to the manufacturer's protocol. The samples were detected by Western blotting. The primary antibodies (Myc-Tag (71D10) Rabbit mAb (1: 5,000, Cell Signaling Technology, 2278S), DYKDDDDK Tag Antibody (1: 5,000, Cell Signaling Technology, 2368S) and β-Tubulin Monoclonal Antibody (1: 10,000, Gene-Protein Link, P01L06)) and the secondary

antibodies (Goat Anti-Rabbit IgG-HRP (1:10,000) and Goat Anti-Mouse IgG-HRP (1:10,000)) were used for immunoblots.

EPAS1 expression knockdown by RNAi

RNAi was used to knock down *EPAS1* gene expression in 293T cells. *EPAS1* short interfering RNA (siRNA) was transfected using the Lipofectamine RNAiMAX Reagent (Invitrogen) according to the manufacturer's instructions. Total RNA was extracted from 293T cells after 48 h of culture in a $\rm CO_2$ incubator, following the extraction protocol described above for liver samples. The cDNA sequences were synthesized using the PrimeScript reverse transcriptase and subsequently used for qPCR with the TB Green Premix Ex Taq II kit (Takara) according to the manufacturer's instructions. qPCR was performed using the LightCycler 480 system (Roche). Relative expression levels of mRNA were calculated using the $\rm \Delta\Delta Ct$ method⁸⁰. The primers used in the experiment are provided in the supplementary material (Supplementary Table 4).

Profiling of metabolites from mouse liver samples using UPLC-MS/MS

A total of 80 whole liver samples were collected from mutant and wild type mice under normoxic (D0) and hypoxic (D2, D3, D4, D7) conditions - eight individuals of each type of mouse at each treatment time point. The samples were stored at -80 °C. Each sample was thawed on ice, cut into small pieces (<1 cm3) on a petri dish. After randomly multipoint sampling, 20 mg of each sample was collected and placed in a 1.5 ml Eppendorf tube, homogenized with steel beads and centrifuged at 1000 g for 30 s at 4 °C. For hydrophilic compounds, we added 400 µl methanol/water (7:3, vol/vol) solution containing an internal standard mixture (Supplementary Table 5) to the Eppendorf tube. The mixture was shaken at 500 g for 5 min and incubated on ice for 15 min. The samples were then centrifuged at 12,400 g for 10 min at 4 °C. We transferred 300 µl of the supernatant to a new Eppendorf tube and placed the samples at -20 °C for 30 min. After centrifugation, the supernatant (200 ul) was used for the widely targeted metabolomic analysis. For hydrophobic compounds extraction, we added 1 ml methyl-tert-butyl ether: methanol (3:1, vol/vol) solution containing an internal standard mixture (Supplementary Table 6) to the Eppendorf tube. After vortexing the mixture for 15 min, 200 µl of water was added, swirled for 1 min and centrifuged at 12,400 g for 10 min at 4 °C. The upper organic layer (200 µl) was collected and dried, followed by a reconstitution using 200 µl of acetonitrile/isopropanol (10:90, vol/vol; mobile phase B) and used for widely targeted lipidomics.

Quality control (QC) samples were constituted by mixing equal volumes of all liver samples with the internal standard mixture. During UPLC-MS/MS detection, QC samples were analyzed after every ten tests to verify the repeatability of the experimental assay. Pearson correlation analysis was performed on the QC samples. The higher the correlation between the QC samples (r^2 closer to 1), the better the stability of the entire testing process, indicating a higher data quality. In addition, we also estimated the degree of data dispersion through calculating the coefficient of variation (CV) values, which is the ratio of the standard deviation from the mean of the data. A higher proportion of metabolites with lower CV values in the QC samples indicates a greater experimental data stability. We here followed a previous protocol⁸¹, considering the experimental data to be (a) 'relatively stable' when the proportion of metabolites with CV ≤ 0.5 in the QC samples was above 85%; and (b) as 'highly stable' when the proportion of metabolites with CV ≤ 0.3 exceeded 75% (Supplementary Figs. 42-44).

Hydrophilic compound extracts were analyzed using the liquid chromatography electrospray ionization tandem mass spectrometry (LC-ESI-MS/MS), which includes the ultra-performance liquid chromatography (UPLC; ExionLC AD) and tandem mass spectrometry (MS/MS; QTRAP). The UPLC conditions were set as follows: the Waters

ACQUITY UPLC HSS T3 C18 column (1.8 µm, 2.1 mm*100 mm); solvent system comprising water (mobile phase A) and acetonitrile (mobile phase B), both of which contained 0.1% formic acid; gradient program (mobile phase A/B) 95:5 (vol/vol) at 0 min, 10:90 (vol/vol) at 11 min, 10:90 (vol/vol) at 12 min, 95:5 (vol/vol) at 12.1 min, 95:5 (vol/vol) at 14 min; flow rate 0.4 ml/min; column temperature was 40 °C; injection volume 2 µl. In addition, the MS was conducted with the conditions: electrospray ionization temperature at 500 °C; ion spray voltage 5500 V for positive and 4500 V for negative; ion source gas I, gas II and curtain gas set to 55, 60, and 25 psi, respectively; collision gas set to high.

Hydrophobic compound extracts were analyzed by the LC-ESI-MS/MS analysis. The UPLC conditions were set as follows: the Thermo Accucore $^{\text{\tiny TM}}$ C30 column (2.6 µm, 2.1 mm*100 mm i.d.); solvent system comprising acetonitrile/water (60:40, vol/vol; mobile phase A) and acetonitrile/isopropanol (10:90, vol/vol; mobile phase B), both of which contained 0.1% formic acid and 10 mmol/L ammonium formate; gradient program (mobile phase A/B) 80:20 (vol/vol) at 0 min, 70:30 (vol/vol) at 2 min, 40:60 (vol/vol) at 4 min, 15:85 (vol/vol) at 9 min, 10:90 (vol/vol) at 14 min, 5:95 (vol/vol) at 17.3 min, 80:20 (vol/vol) at 20 min; flow rate 0.35 ml/min; column temperature 45 °C; injection volume 2 µl. In addition, the MS was conducted with the conditions: electrospray ionization temperature at 500 °C; ion spray voltage 5500 V for positive and 4500 V for negative; ion source gas I, gas II and curtain gas set to 45, 55, and 35 psi, respectively; collision gas set to medium.

We identified the metabolites based on their retention time (RT), ion pair information and secondary spectrum data using the Metware metabolite database (MWDB)⁴⁵, and the metabolites were quantified using multiple reaction monitoring of the triple quadrupole mass spectrometer. We integrated and corrected the mass spectrum peaks of the same metabolites from different samples after the peaks were integrated by peak areas. Using Metware's intelligent secondary spectrum matching method, the secondary spectrum and RT of metabolites in the samples were compared and intelligently matched against the secondary spectrum and RT in the MWDB⁸². The data quality was first assessed by the Pearson correlation coefficients (PCC) between control samples using cor function in R (version 3.5.1), and CV values were estimated. The PCA was performed using the prcomp function with unit variance scaling in R (version 3.5.1). OPLS-DA was conducted using the MetaboAnalystR (version 1.0.1) package in R with a log transformed and zero-centered dataset. A permutation test (n = 200) was performed to avoid overfitting. Variable importance in projection (VIP) values were obtained from the OPLS-DA analysis. Significantly regulated metabolites in *EPAS1**/+ and *EPAS1*V162T/V162T mice under normoxic or hypoxic conditions were determined by VIP≥1 and fold change ≥ 1.5 or ≤ 0.67 . Identified metabolites were annotated according to the KEGG Compound database (http://www.kegg.jp/ kegg/compound/) and then mapped to the KEGG Pathway database (http://www.kegg.jp/kegg/pathway.html). P values were required to be less than 0.05.

To verify the differentially expressed metabolites between mutant and wild type mice detected using the widely targeted metabolomics analysis, we checked the main fuels (e.g., glucose, Lauric acid (12:0)) for glucose and lipid metabolism at the key time points in our study using the targeted metabolomic analysis. We randomly selected liver samples followed a multi-point sampling method described above and added the external standards (Supplementary Table 7). For the glucose content detection (mutant vs wild type mice individuals: 3 vs 3 on D4 and D7), 50 mg of each sample was added to a solution of 500 μ l methanol/water (7:3, vol/vol), vortexed for 3 min, and centrifuged at 12,400 g for 10 min at 4 °C. The 300 μ l of supernatant was collected and incubated at -20 °C for 30 min. After centrifugation, 200 μ l of supernatant was used for the LC-MS/MS analysis 53. For the FFA content detection (mutant vs wild type mice individuals: 5 vs 5

on D3 and D4), 50 mg of each sample was added to a solution containing 150 μ l methanol, 200 μ l methyl-tert-butyl ether and 50 μ l 36% phosphoric acid/ water (vol/vol), vortexed for 3 min and then centrifuged at 12,400 g for 5 min at 4 °C. The 200 μ l of supernatant was collected and dried. The dried sample was added to 300 μ l 15% boron trifluoride methanol (vol/vol) solution, vortexed for 3 min, incubated 30 min at 60 °C, cooled to room temperature and added to a mixture of 500 μ l n-hexane solution and 200 μ l saturated sodium chloride solution. After vortexing and centrifuging, the 100 μ l of supernatant was used for the GC-MS/MS analysis 84. With identification, quantification and data quality assessment, the significantly regulated metabolites between mutant and wild type mice were determined by VIP \geq 1 and fold change \geq 1.5 or \leq 0.67.

Metabolite profiling of saker blood samples using UPLC-MS/MS Since the saker falcon is an endangered animal species listed in the CITES Appendix I, it is ethically essentially impossible to do liver metabolite profiling on wild sakers. Nonetheless, previous studies have suggested that liver metabolism has an important impact on blood metabolite levels Es. We therefore chose to study the plasma, to minimize the sampling disturbance and to check the metabolic characteristics of wild sakers. As for potential dietary effects on the organism's glucose and lipid metabolism, we chose to randomly capture them in our experimental grid on the QTP. We collected a total of ten plasma samples (from six homozygous mutants and four heterozygous mutants) from wild sakers possessing the *EPAS1* allele. 200 μ l of blood was collected from each individual using an EDTA-anticoagulant vacuum tube, transferred to a 1.5 ml Eppendorf tube and centrifuged at 200 g for 10 min at 4 °C. The supernatant plasma samples were col-

lected and stored at -80 °C.

Each sample was thawed on ice and vortexed for 10 s. For hydrophilic compound extracts, we transferred 50 µl plasma to 300 µl of an acetonitrile/methanol (1:4, vol/vol) solution containing an internal standard mixture (Supplementary Table 8) in an Eppendorf tube. The mixture was vortexed for 3 min and then centrifuged at 12,400 g for 10 min at 4 °C. We transferred 200 µl of supernatant to a new Eppendorf tube and placed the samples at -20 °C for 30 min. After centrifugation, the supernatant (180 µl) was used for widely targeted metabolomic analysis. For hydrophobic compound extracts, we transferred 50 µl of plasma and added 1 ml methyl-tertbutyl ether: methanol (3:1, vol/vol) solution containing an internal standard mixture (Supplementary Table 9) to the Eppendorf tube. After vortexing for 15 min, 200 µl of water was added, swirled for 1 min and centrifuged at 12,400 g for 10 min at 4 °C. The upper organic layer (200 µl) was collected and dried, followed by a reconstitution using 200 µl of acetonitrile/isopropanol (1:1, vol/vol) and transferred for widely targeted lipidomics. The metabolite identification, quantification and data quality assessment followed the protocol described above. Significantly regulated metabolites between homozygous and heterozygous saker genotypes were determined by VIP ≥ 1 and p value < 0.05.

Both hydrophilic and hydrophobic compound extracts were also analyzed by the LC-ESI-MS/MS. Pearson correlation analysis was performed on the QC samples showed a higher correlation between the QC samples (r^2 closer to 1), and the proportion of metabolites with CV \leq 0.3 exceeds 75%, indicating the experimental data is highly stable (Supplementary Fig. 45). The metabolite identification, quantification, data quality assessment and significance determination again followed the protocol described above.

Identification of the full-length transcripts

We performed an Iso-seq to obtain full-length transcripts of *EPAS1* gene. The liver samples were collected from mutant and wild type mice under normoxic (n = 8 vs 8 on D0) and hypoxic conditions (10 vs 10 on D2, 6 vs 10 on D3, 12 vs 10 on D4 and 9 vs 9 on D7). We pooled RNA

extracts (TRIzol method) from the two types of mice, constructed transcriptomic libraries and subjected them to the PacBio Sequel II (PacBio) platform for sequencing⁸⁶. The generated raw sequences were proceeded to capture circular consensus sequencing (CCS) reads using the CCS program in *smrtlink* (https://www.pacb.com/support/ software-downloads/, version 11.0) with parameters "--min-passes 0 --min-length 50 --max-length 50000 --min-rq 0.75 -j 15". The CCS data were aligned with sequencing primer sequences using BLAST (version 2.2.26)87 and sorted using a customized script classify_by_primer.pl (parameters: -umilen 8 -min primerlen 16 -min isolen 100; https:// github.com/shizhuoxing/BGI-Full-Length-RNA-Analysis-Pipeline) produce full length non-chimeric reads (FLNC). The FLNCs were aligned with the Mus musculus genome (mm39) using Minimap2 (version 2.13)⁸⁸. After filtering low-quality mapping reads (PHRED < 10) and removing duplicates using Samtools (version 1.9)89, we identified the gene isoforms using cDNA_Cupcake (https://github.com/Magdoll/ cDNA Cupcake, version 5.8) with parameters "-c 0.95 -i 0.95 --dunmerge-5-shorter".

Identification of differentially expressed transcripts and genes

We collected liver samples from mutant and wild type mice under normoxic (n = 8 vs 8 on D0) and hypoxic treatments (10 vs 10 on D2, 6 vs 10 on D3, 12 vs 10 on D4 and 9 vs 9 on D7) for transcriptomic analysis. Six to ten individuals were randomly selected from each group for RNA-seq library construction followed by a sequencing on a BGISEQ-500 sequencing platform (The Beijing Genomics Institute). Raw data were filtered using $SOAPnuke^{90}$ with parameters "-n 0.01 -i 20 -q 0.4 -adaMR 0.25 --ada_trim --polyX 50 --minReadLen 150". Clean reads were aligned with transcripts from the whole mouse genome annotation and Iso-Seq using Bowtie2 (version 2.3.4.3)⁹¹. The expression level of each transcript was quantified as transcripts per million (TPM) with counts using transcripts per million (TPM) with counts using transcripts per million (TPM) with counts using transcripts per million (TPM)

The differentially expressed transcript (DET) was detected following our published pipeline²⁸. We used three types of software - *edgeR* (version 3.40.2)⁹³, *DESeq2* (version 1.38.3)⁹⁴ and *limma* (version 3.54.2)⁹⁵ - to identify DETs. *P* values were adjusted using the FDR method. A transcript was identified as a DET when it was supported by more than two different methods, the fold change was required $\log_2 FC \mid \ge 0.26$ and *q* value was less than 0.05.

The expression level of each gene was then quantified by aggregating the expression of all transcripts belonging to the same gene, and DEGs were identified following the same pipeline used for the DET detection. The volcano plots were created using the *ggplot2* package in *R* (version 4.3.2). KEGG enrichment of DEGs was conducted using *clusterProfiler* (version 4.6.2)⁹⁶. The enriched KEGG pathways were excluded if the gene number was less than three. *P* values were adjusted by the FDR method and were required to be less than 0.05 after adjustment.

Differential gene regulatory network construction

We constructed the gene interaction network using an SSN method 97 . We calculated the Pearson correlation coefficients between expression levels of genes in the wild type and mutant type mice to construct a control network and a case network, respectively. The differential network was then calculated using the difference between the case and control networks. We finally obtained the differential networks between the two groups of mice with significant difference (p < 0.05).

We mapped the identified differential networks between the two groups of mice at D0, D2, D3, D4, D7 to the constructed gene regulatory network database⁹⁸ which combines the information from BioGRID (http://thebiogrid.org/), Ensembl (http://www.ensembl.org), FANTOM, GenBank (http://www.ncbi.nlm.nih.gov/genbank/), RefSeq (http://www.ncbi.nlm.nih.gov/refseq/), STRING, TRANSFAC (http://www.gene-regulation.com/pub/databases.html), IntAct, JASPAR and

KEGG. We used the relationships between transcription factors themselves and between transcription factors and their target genes to obtain gene regulatory networks for each experimental treatment.

We explored the regulatory relationship of genes involved in glucose metabolism and lipid metabolism and obtained the subnetworks of gene regulation directly involved in each metabolism mode. Similarly, a subnetwork of *EPAS1* gene regulation was identified. We integrated the nodes on subnetworks and selected the shortest road between the *EPAS1* gene and downstream regulated genes related to glucose and lipid metabolism. The final subnetworks were visualized using *Gephi* (version 0.10.1)⁹⁹.

Structural equation model simulations

We constructed a structural equation model with four variables genetic factors (*G*), environmental factors (*E*), genetic and environmental interaction (*GtE*) and behavioral factors (*B*) - in order to investigate the contribution of each variable to the RER using the *lavaan* program (version 0.6.15) in *R*. First, we averaged the RER for each individual under normoxia (D0) and hypoxia (D2, D3, D4, D7) and used this as the RER value of the tested group. A total of 16 observations were used for model construction. Second, we used PCA to downscale the four behavioral factors (breathing rate, food intake, food absorption ((1- (fecal mass/ food intake)) *100) and locomotion) and used the PC1 as a proxy for the behavioral changes. We then constructed the SEM model using these equations:

$$RER = \alpha_{RER} + \beta_{RER_G} \times G + \beta_{RER_F} \times E + \beta_{RER_{GFF}} \times GtE + \beta_{RER_B} \times B$$
 (1)

where α_{RER} is intercept, β_{RER_G} a genetic factor, β_{RER_E} an environmental factor, $\beta_{RER_{GLE}}$ a factor of genetic and environmental interaction, and β_{RER_B} a behavioral factor.

Behavior was also assumed to be influenced by genetic, environmental, and genetic and environmental interaction variables:

$$B = \alpha_B + \beta_{B_C} \times G + \beta_{B_E} \times E + \beta_{B_{CE}} \times GtE$$
 (2)

where the interaction of genetic and environment was noted as:

$$GtE = G \times E \tag{3}$$

For all calculations, the genetic and environment variables were set to 1 and 2, denoting *EPAS1*^{V162T}/*versus* wild type, and hypoxia *versus* normoxia, respectively:

$$E, G \in \{0, 1\}$$

Estimation of survival rate under acute hypoxia

The neck hair of mutant (n=30) and wild type mice (n=30) were removed three days prior to treatment. We measured the heart rate of each individual using the MouseOx Plus pulse oximeter through a collar clip. The measurement was conducted in a non-invasive manner and in real time, according to our previously established protocol⁹. After the mice had acclimated to the clip for 1–2 h, they were preacclimated to different oxygen concentrations (21% O_2 , 15% O_2 and 10% O_2) prior to acute hypoxia exposure, with 10 min intervals allowed for acclimation under each treatment. Heart rate measurement began when the oxygen concentration was decreased to 10% and 4%. The heart rate was then continuously monitored until the signal ceased, which was considered to be the end of life¹⁰⁰.

Statistical analysis

Unless stated otherwise, *p* values were calculated using Student's *t* tests (two-sided).

Reporting summary

Further information on research design is available in the Nature Portfolio Reporting Summary linked to this article.

Data availability

All RNA-seq and Iso-seq data generated in this study have been deposited in the GSA database under accession code PRJCA033928. The metabolomics and lipidomics data generated in this study have been deposited in the OMIX database under accession code OMIX011636. The *Mus musculus* genome and gene annotation for RNA-seq and Iso-seq analyses used in this study is available in the NCBI database under accession code GCF_000001635.27 [https://www.ncbi.nlm.nih.gov/datasets/genome/GCF_000001635.27/]. Source data are provided with this paper.

Code availability

The *smrtlink* package used to capture CCS reads is publicly available at https://www.pacb.com/support/software-downloads/. The script (classify_by_primer.pl) for CCS data alignment is publicly available and has been deposited in GitHub at https://github.com/shizhuoxing/BGI-Full-Length-RNA-Analysis-Pipeline. The *cDNA_Cupcake* package for isoform identification is publicly available and has been deposited in GitHub at https://github.com/Magdoll/cDNA_Cupcake. No novel algorithms or reusable software packages were developed for this study.

References

- 1. Cannon, W. B. Organization for physiological homeostasis. *Physio. Rev.* **9**, 399–431 (1929).
- Benzinger, T. H. Heat regulation: homeostasis of central temperature in man. *Physio. Rev.* 49, 671–759 (1969).
- Fitzsimons, J. T. Evolution of physiological and behavioural mechanisms in vertebrate body fluid homeostasis. In *Thirst: Phy*siological and Psychological Aspects (Springer, 1991).
- Yu, S. B. & Pekkurnaz, G. Mechanisms orchestrating mitochondrial dynamics for energy homeostasis. *J. Mol. Biol.* 430, 3922–3941 (2018).
- 5. Pi, X., Xie, L. & Patterson, C. Emerging roles of vascular endothelium in metabolic homeostasis. *Circ. Res.* **123**, 477–494 (2018).
- Beall, C. M. Two routes to functional adaptation: Tibetan and Andean high-altitude natives. *Proc. Natl. Acad. Sci. USA* 104, 8655–8660 (2007).
- 7. Ortiz-Prado, E., Dunn, J. F., Vasconez, J., Castillo, D. & Viscor, G. Partial pressure of oxygen in the human body: a general review. *Am. J. Blood Res.* **9**, 1–14 (2019).
- Laguë, S. L. High-altitude champions: birds that live and migrate at altitude. J. Appl. Physiol. 123, 942–950 (2017).
- Hu, L. et al. Arctic introgression and chromatin regulation facilitated rapid Qinghai-Tibet Plateau colonization by an avian predator. *Nat. Commun.* 13, 6413 (2022).
- Chawla, S. & Saxena, S. Physiology of high-altitude acclimatization. Resonance. 19, 538–548 (2014).
- 11. Moore, L. G., Fernando Armaza, V., Villena, M. & Vargas, E. Comparative aspects of high-altitude adaptation in human populations. *Adv. Exp. Med. Biol.* **475**, 45–62 (2022).
- Storz, J. F. Hemoglobin function and physiological adaptation to hypoxia in high-altitude mammals. J. Mammal. 88, 24–31 (2007).
- Xu, D. et al. A single mutation underlying phenotypic convergence for hypoxia adaptation on the Qinghai-Tibetan Plateau. *Cell Res.* 31, 1032–1035 (2021).
- O'Brien, K. A., Simonson, T. S. & Murray, A. J. Metabolic adaptation to high altitude. Curr. Opin. Endocr. Metab. Res. 11, 33–41 (2020).
- Heimbucher, T., Hog, J., Gupta, P. & Murphy, C. T. PQM-1 controls hypoxic survival via regulation of lipid metabolism. *Nat. Commun.* 11, 4627 (2020).

- Polan, D. M., Alansari, M., Lee, B. & Grewal, S. S. Early-life hypoxia alters adult physiology and reduces stress resistance and lifespan in Drosophila. J. Exp. Biol. 223, jeb226027 (2020).
- 17. Leverve, X., Batandier, C. & Fontaine, E. Choosing the right substrate. In Sepsis: New Insights, New Therapies: Novartis Foundation Symposium. (Wiley, 2007).
- Ge, R. L. et al. Draft genome sequence of the Tibetan antelope. Nat. Commun. 4, 1858 (2013).
- Cheviron, Z. A., Bachman, G. C., Connaty, A. D., McClelland, G. B. & Storz, J. F. Regulatory changes contribute to the adaptive enhancement of thermogenic capacity in high-altitude deer mice. *Proc. Natl. Acad. Sci. USA* 109, 8635–8640 (2012).
- Qu, Y. et al. Ground tit genome reveals avian adaptation to living at high altitudes in the Tibetan plateau. *Nat. Commun.* 4, 2071 (2013).
- Schippers, M. P., Ramirez, O., Arana, M., Pinedo-Bernal, P. & McClelland, G. B. Increase in carbohydrate utilization in highaltitude Andean mice. Curr. Biol. 22, 2350–2354 (2012).
- Randle, P. J. Regulatory interactions between lipids and carbohydrates: the glucose fatty acid cycle after 35 years. *Diabetes Metab. Rev.* 14, 263–283 (1998).
- 23. Pan, S. et al. Convergent genomic signatures of flight loss in birds suggest a switch of main fuel. *Nat. Commun.* **10**, 2756 (2019).
- Luo, X. et al. Reducing VEGFB expression regulates the balance of glucose and lipid metabolism in mice via VEGFR1. *Mol. Med. Rep.* 26, 285 (2022).
- Yang, Y., Wu, Y., Sun, X. D. & Zhang, Y. Reactive oxygen species, glucose metabolism, and lipid metabolism. Oxidative Stress: Human Diseases and Medicine, 213-235 (Springer, 2021).
- Yi, X. et al. Sequencing of 50 human exomes reveals adaptation to high altitude. Science 329, 75–78 (2010).
- Li, Y. et al. Population variation revealed high-altitude adaptation of Tibetan mastiffs. Mol. Biol. Evol. 31, 1200–1205 (2014).
- Pan, S. et al. Population transcriptomes reveal synergistic responses of DNA polymorphism and RNA expression to extreme environments on the Qinghai-Tibetan Plateau in a predatory bird. Mol. Ecol. 26, 2993–3010 (2017).
- Ortmann, B., Druker, J. & Rocha, S. Cell cycle progression in response to oxygen levels. *Cell. Mol. Life Sci.* 71, 3569–3582 (2014).
- 30. Liu, Y. et al. HIF-1 α and HIF-2 α are critically involved in hypoxia-induced lipid accumulation in hepatocytes through reducing PGC-1 α -mediated fatty acid β -oxidation. *Toxicol. Lett.* **226**, 117–123 (2014).
- 31. Du, W. et al. HIF drives lipid deposition and cancer in ccRCC via repression of fatty acid metabolism. *Nat. Commun.* **8**, 1769 (2017).
- Ramakrishnan, S. K. & Shah, Y. M. A central role for hypoxiainducible factor (HIF)–2α in hepatic glucose homeostasis. *Nutr. Healthy Aging* 4, 207–216 (2017).
- Woolcott, O. O., Ader, M. & Bergman, R. N. Glucose homeostasis during short-term and prolonged exposure to high altitudes. *Endocr. Rev.* 36, 149–173 (2015).
- Gaspar, J. M. & Velloso, L. A. Hypoxia inducible factor as a central regulator of metabolism-implications for the development of obesity. Front. Neurosci. 12, 813 (2018).
- Li, C. et al. Genetic changes in the *EPAS1* gene between Tibetan and Han ethnic groups and adaptation to the plateau hypoxic environment. *PeerJ* 7, e7943 (2019).
- Chen, Y., Jiang, C., Luo, Y., Liu, F. & Gao, Y. An EPAS1 haplotype is associated with high altitude polycythemia in male Han Chinese at the Qinghai-Tibetan plateau. Wild. Environ. Med. 25, 392–400 (2014)
- Pan, W. et al. Association between single nucleotide polymorphisms in *PPARA* and *EPAS1* genes and high-altitude appetite loss in Chinese young men. *Front. Physiol.* 10, 59 (2019).

- Majmundar, A. J., Wong, W. J. & Simon, M. C. Hypoxia-inducible factors and the response to hypoxic stress. *Mol. Cell* 40, 294–309 (2010).
- Wu, X. Y. et al. Novel SNP of *EPAS1* gene associated with higher hemoglobin concentration revealed the hypoxia adaptation of yak (Bos grunniens). J. Integr. Agr. 14, 741–748 (2015).
- Li, J. T. et al. Comparative genomic investigation of high-elevation adaptation in ectothermic snakes. *Proc. Natl. Acad. Sci. USA* 115, 8406–8411 (2018).
- 41. Hall, B. et al. Genome editing in mice using CRISPR/Cas9 technology. *Curr. Protoc. Cell Biol.* **81**, e57 (2018).
- 42. Vanderhaeghen, T., Beyaert, R. & Libert, C. Bidirectional crosstalk between hypoxia inducible factors and glucocorticoid signaling in health and disease. *Front. Immunol.* **12**, 684085 (2021).
- Pan, Q. et al. Lipidomics reveals mitochondrial membrane remodeling associated with acute thermoregulation in a rodent with a wide thermoneutral zone. *Lipids* 49, 715–730 (2014).
- 44. Jeukendrup, A. E. & Wallis, G. A. Measurement of substrate oxidation during exercise by means of gas exchange measurements. *Int. J. Sports Med.* **26**, S28–S37 (2005).
- Liu, J. et al. Metabolite profile of COVID-19 revealed by UPLC-MS/ MS-based widely targeted metabolomics. Front. Immunol. 13, 894170 (2022).
- 46. Kim, H. O., Jo, Y. H., Lee, J., Lee, S. S. & Yoon, K. S. The C1772T genetic polymorphism in human HIF-1α gene associates with expression of HIF-1α protein in breast cancer. Oncol. Rep. 20, 1181–1187 (2008).
- Peng, Y. et al. Down-regulation of EPAS1 transcription and genetic adaptation of Tibetans to high-altitude hypoxia. Mol. Biol. Evol. 34, 818–830 (2017).
- Carr, R. M. & Ahima, R. S. Pathophysiology of lipid droplet proteins in liver diseases. Exp. Cell Res. 340, 187–192 (2016).
- Itabe, H., Yamaguchi, T., Nimura, S. & Sasabe, N. Perilipins: a diversity of intracellular lipid droplet proteins. *Lipids Health Dis*. 16. 1–11 (2017).
- 50. Huh, J. Y. et al. TANK-binding kinase 1 regulates the localization of acyl-CoA synthetase ACSL1 to control hepatic fatty acid oxidation. *Cell Metab.* **32**, 1012–1027 (2020).
- 51. Rankin, E. B. et al. Hypoxia-inducible factor 2 regulates hepatic lipid metabolism. *Mol. Cell Biol.* **29**, 4527–4538 (2009).
- 52. Metallo, C. M. et al. Reductive glutamine metabolism by IDH1 mediates lipogenesis under hypoxia. *Nature* **481**, 380–384 (2012).
- Ivy, C. M. & Scott, G. R. Control of breathing and the circulation in high-altitude mammals and birds. Comp. Biochem. Physiol. A Mol. Integr. Physiol. 186, 66–74 (2015).
- 54. Scott, G. R. & Milsom, W. K. Control of breathing and adaptation to high altitude in the bar-headed goose. *Am. J. Physiol. Regul. Integr. Comp. Physiol.* **293**, R379–R391 (2007).
- Zhang, X. et al. A high altitude respiration and SpO2 dataset for assessing the human response to hypoxia. Sci. Data 11, 248 (2024).
- Lau, D. S. et al. Acclimation to hypoxia increases carbohydrate use during exercise in high-altitude deer mice. Am. J. Physiol. Regul. Integr. Comp. Physiol. 312, R400–R411 (2017).
- Pagano, A. M. et al. Polar bear energetic and behavioral strategies on land with implications for surviving the ice-free period. *Nat. Commun.* 15, 947 (2024).
- Kayser, B. & Verges, S. Hypoxia, energy balance and obesity: from pathophysiological mechanisms to new treatment strategies.
 Obes. Rev. 14, 579–592 (2013).
- Cabrera-Aguilera, I. et al. Additive effects of intermittent hypobaric hypoxia and endurance training on bodyweight, food intake, and oxygen consumption in rats. *High. Alt. Med. Biol.* 19, 278–285 (2018).
- 60. Ward, N. L. et al. Cerebral angiogenic factors, angiogenesis, and physiological response to chronic hypoxia differ among four

- commonly used mouse strains. J. Appl. Physiol. **102**, 1927–1935 (2007).
- 61. Rui, L. Energy metabolism in the liver. *Compr. Physiol.* **4**, 177 (2014).
- Sevastianova, K. et al. Effect of short-term carbohydrate overfeeding and long-term weight loss on liver fat in overweight humans123. Am. J. Clin. Nutr. 96, 727–734 (2012).
- Suter, P. M., Schutz, Y. & Jequier, E. The effect of ethanol on fat storage in healthy subjects. N. Engl. J. Med. 326, 983–987 (1992).
- 64. Roh, L. et al. Mortality risk associated with underweight: a censuslinked cohort of 31,578 individuals with up to 32 years of follow-up. BMC Public Health 14, 371 (2014).
- Tannheimer, M. et al. Changes of hematocrit and hemoglobin concentration in the cold Himalayan environment in dependence on total body fluid. Sleep. Breath. 14, 193–199 (2010).
- Stobdan, T. et al. Endothelin receptor B, a candidate gene from human studies at high altitude, improves cardiac tolerance to hypoxia in genetically engineered heterozygote mice. *Proc. Natl.* Acad. Sci. USA 112, 10425–10430 (2015).
- Park, T. J. et al. Fructose-driven glycolysis supports anoxia resistance in the naked mole-rat. Science 356, 307–311 (2017).
- 68. Gonzalez, F. J., Xie, C. & Jiang, C. The role of hypoxia-inducible factors in metabolic diseases. *Nat. Rev. Endocrinol.* **15**, 21–32 (2019).
- Peng, J., Zhang, L., Drysdale, L. & Fong, G. H. The transcription factor EPAS-1/hypoxia-inducible factor 2α plays an important role in vascular remodeling. *Proc. Natl. Acad. Sci. USA* 97, 8386–8391 (2000).
- Ghalehbandi, S., Yuzugulen, J., Pranjol, M. Z. I. & Pourgholami, M. H. The role of VEGF in cancer-induced angiogenesis and research progress of drugs targeting VEGF. Eur. J. Pharmacol. 949, 175586 (2023).
- Yu, T., Tang, B. & Sun, X. Development of inhibitors targeting hypoxia-inducible factor 1 and 2 for cancer therapy. *Yonsei Med. J.* 58, 489–496 (2017).
- Chen, J. et al. Hypoxia exacerbates nonalcoholic fatty liver disease via the HIF-2α/PPARα pathway. Am. J. Physiol. Endocrinol. Metab. 317, E710–E722 (2019).
- Xie, Z. et al. Integration of proteomics and metabolomics reveals energy and metabolic alterations induced by glucokinase (GCK) partial inactivation in hepatocytes. Cell Signal. 114, 111009 (2024).
- Yang, Y. et al. The multi-omics analyses of acsl1 reveal its translational significance as a tumor microenvironmental and prognostic biomarker in clear cell renal cell carcinoma. *Diagn. Pathol.* 18, 96 (2023).
- Speakman, J. R. Measuring energy metabolism in the mousetheoretical, practical, and analytical considerations. Front. Physiol. 4, 34 (2013).
- Concordet, J. P. & Haeussler, M. CRISPOR: intuitive guide selection for CRISPR/Cas9 genome editing experiments and screens. Nucleic Acids Res. 46, W242–W245 (2018).
- R Core Team. R: A language and environment for statistical computing. (2013).
- Bates, D., Mächler, M., Bolker, B. & Walker, S. Fitting linear mixedeffects models using lme4. J. Stat. Softw. 67, 1–48 (2015).
- Liu, Z. et al. Supplementation with Chinese herbal preparations protect the gut-liver axis of Hu sheep, promotes gut-liver circulation, regulates intestinal flora and immunity. Front. Immunol. 15, 1454334 (2024).
- Livak, K. J. & Schmittgen, T. D. Analysis of relative gene expression data using real-time quantitative PCR and the 2 – ΔΔCT method. Methods 25, 402–408 (2001).
- 81. Hao, M. et al. Widely targeted metabolomic analysis reveals metabolite changes induced by incorporating black tea

- fermentation techniques in oolong tea processing for quality improvement. *Food Chem.* **459**. 140433 (2024).
- 82. Yang, H. et al. Nitrogen nutrition contributes to plant fertility by affecting meiosis initiation. *Nat. Commun.* **13**, 485 (2022).
- Wang, C. et al. ENO2-derived phosphoenolpyruvate functions as an endogenous inhibitor of HDAC1 and confers resistance to antiangiogenic therapy. *Nat. Metab.* 5, 1765–1786 (2023).
- 84. Li, H. et al. CRISPR/Cas9 Screens Reveal that Hexokinase 2 Enhances Cancer Stemness and Tumorigenicity by Activating the ACSL4-Fatty Acid β-Oxidation Pathway. Adv. Sci. 9, 2105126 (2022).
- Shin, S. Y. et al. An atlas of genetic influences on human blood metabolites. *Nat. Genet.* 46, 543–550 (2014).
- 86. Wang, B. et al. A comparative transcriptional landscape of maize and sorghum obtained by single-molecule sequencing. *Genome Res.* **28**, 921–932 (2018).
- 87. Altschul, S. F. et al. Gapped BLAST and PSI-BLAST: a new generation of protein database search programs. *Nucleic Acids Res.* **25**, 3389–3402 (1997).
- 88. Li, H. Minimap2: pairwise alignment for nucleotide sequences. *Bioinformatics* **34**, 3094–3100 (2018).
- 89. Li, H. et al. The sequence alignment/map format and SAMtools. *Bioinformatics* **25**, 2078–2079 (2009).
- Chen, Y. et al. SOAPnuke: a MapReduce accelerationsupported software for integrated quality control and preprocessing of high-throughput sequencing data. *Gigascience* 7, gix120 (2018).
- 91. Langmead, B. & Salzberg, S. L. Fast gapped-read alignment with Bowtie 2. *Nat. Methods* **9**, 357–359 (2012).
- Li, B. & Dewey, C. N. RSEM: accurate transcript quantification from RNA-Seq data with or without a reference genome. *BMC Bioinf.* 12, 1–16 (2011).
- 93. Zhou, X., Lindsay, H. & Robinson, M. D. Robustly detecting differential expression in RNA sequencing data using observation weights. *Nucleic Acids Res.* **42**, e91–e91 (2014).
- 94. Love, M. I., Huber, W. & Anders, S. Moderated estimation of fold change and dispersion for RNA-seq data with DESeq2. *Genome Biol.* **15**, 550 (2014).
- Ritchie, M. E. et al. limma powers differential expression analyses for RNA-sequencing and microarray studies. *Nucleic Acids Res.* 43, e47–e47 (2015).
- 96. Yu, G., Wang, L. G., Han, Y. & He, Q. Y. clusterProfiler: an R package for comparing biological themes among gene clusters. *Omics J. Integr. Biol.* **16**, 284–287 (2012).
- Liu, Z. P., Wu, C., Miao, H. & Wu, H. RegNetwork: an integrated database of transcriptional and post-transcriptional regulatory networks in human and mouse. *Database* 2015, bav095 (2015).
- 98. Liu, X., Wang, Y., Ji, H., Aihara, K. & Chen, L. Personalized characterization of diseases using sample-specific networks. *Nucleic Acids Res.* **44**, e164 (2016).
- Bastian, M., Heymann, S. & Jacomy, M. Gephi: an open source software for exploring and manipulating networks. *ICWSM* 8, 361–362 (2009).
- 100. Gerritzen, M. A., Lambooij, E., Reimert, H. G., Spruijt, B. M. & Stegeman, J. A. Susceptibility of duck and turkey to severe hypercapnic hypoxia. *Poult. Sci.* **85**, 1055–1061 (2006).

Acknowledgements

This study was supported by National Natural Science Foundation of China grants 32125005, 32361133559, T2450075 (to X.Z.), 32222012 (to S.P.), 32370460 (to L.H.), 32070416 (to S.P.), International Partnership Program of Chinese Academy of Sciences for Grand Challenges (073GJHZ2023091GC) (to X.Z.), Royal Society International Exchanges

grant IEC\NSFC\181744 (to F.H. and X.Z), and the Institute of Zoology, Chinese Academy of Sciences (2023IOZ0104). We thank Drs J.A.M. Graves, D. Raubenheimer for their helpful comments on this study; D.N. Tang and T.X. Zhang for their assistance with data analysis; J.B. Sun, Z.Y. Zhang and F. Li for assistance in the fieldwork and sample collection of saker falcons; Three-River-Source National Park for help in the field; C.B. Chen, Y.B. Chen and C.P. Yang for help with mouse maintenance; S. Hailer for carefully proofreading the revision; X. Hou and X.H. Zhang for their advice on figure drawing.

Author contributions

X.Z. conceived and designed the study. Y.L., B.L., and Z.L. conducted the molecular and animal experiments. Y.L., L.H., X.S., Y.C., S.P., and F.H. performed the data analysis. Z.G. provided the help with statistical analysis and fieldwork. X.Z., L.H., and Y.L. wrote the manuscript, with contributions on data interpretation and writing from F.H.

Competing interests

The authors declare no competing interests.

Additional information

Supplementary information The online version contains supplementary material available at https://doi.org/10.1038/s41467-025-64110-w.

Correspondence and requests for materials should be addressed to Li Hu or Xiangjiang Zhan.

Peer review information *Nature Communications* thanks the anonymous, reviewer(s) for their contribution to the peer review of this work. A peer review file is available.

Reprints and permissions information is available at http://www.nature.com/reprints

Publisher's note Springer Nature remains neutral with regard to jurisdictional claims in published maps and institutional affiliations.

Open Access This article is licensed under a Creative Commons Attribution-NonCommercial-NoDerivatives 4.0 International License, which permits any non-commercial use, sharing, distribution and reproduction in any medium or format, as long as you give appropriate credit to the original author(s) and the source, provide a link to the Creative Commons licence, and indicate if you modified the licensed material. You do not have permission under this licence to share adapted material derived from this article or parts of it. The images or other third party material in this article are included in the article's Creative Commons licence, unless indicated otherwise in a credit line to the material. If material is not included in the article's Creative Commons licence and your intended use is not permitted by statutory regulation or exceeds the permitted use, you will need to obtain permission directly from the copyright holder. To view a copy of this licence, visit http://creativecommons.org/licenses/by-nc-nd/4.0/.

© The Author(s) 2025